12

Electron Beams in Plasmas

We have looked briefly at plasma properties several times in previous chapters. In this chapter, we shall initiate a more detailed study of plasmas with emphasis on their response to pulsed high-current electron beams. There is a large body of literature on the topic because of the possibility of long-distance propagation of electron beams through the atmosphere and the potential use of intense beams for plasma heating. We shall concentrate on the motion of charged particles rather than the atomic processes involved in the creation of plasmas. The models assume pre-formed plasmas and do not address the involved process of ionization by the beam.

We shall limit attention to infinite plasmas with no applied magnetic field. The ideal plasma responds immediately to a pulsed beam, providing complete neutralization of the beam space-charge and current. Four sections in this chapter review plasma properties that limit their response to changes of charge and current density. Section 12.1 describes how plasma electrons neutralize space-charge by shifting their positions. Residual electric fields depend on the temperature of the electrons. The derivations leads to the Debye scale length. Field cancellation may be incomplete over distance smaller than the Debye length. Section 12.2 reviews electrostatic plasma oscillations. These occur when there is a sudden change in charge density, such as the injection of a beam. The oscillations have a characteristic frequency, the electron plasma frequency ω_{pe}.

Although low-temperature plasmas conduct current, they have a much lower conductivity than metals. Sections 12.5 and 12.6 discusses imperfect conduction in plasmas. Resistive effects modify the distribution of plasma return-current for a pulsed beam. Section 12.5 describes how the inertia of electrons delays the plasma response to rapid changes in current. We derive the magnetic skin depth, a characteristic dimension for cancellation of pulsed magnetic fields in plasmas. Section 12.6 reviews the effect of collisional resistivity in plasmas. Resistivity results in spatial spreading of plasma return current over a cross-section larger than that of the beam. As a result, the magnetic field in the beam volume can provide a self-confined equilibrium.

Section 12.3 extends the theory of plasma oscillations to the transverse motion of beam electrons about a core of immobile ions. We will apply the results in Section 13.7 to the hose instability of an ion-confined electron beam. Section 12.4 covers the space-charge neutralization of a pulsed electron beam. We shall calculate the time-dependent shift of plasma electrons by a direct numerical solution of the non-linear moment equations. The treatment illustrates some methods to solve partial differential equations with computers and shows that neutralization is almost complete is the beam current rise time is much longer than $1/\omega_{pe}$.

Section 12.7 describes propagation of a long pulse length beam in a resistive plasma. At late time the plasma return current covers a larger area than the beam current; therefore, there is a non-zero confining magnetic field in the beam volume. The magnetic deflection of electrons in a charge-neutral beam defines an upper limit on the transportable current. The Alfven current I_A is a useful scaling parameter for intense beam studies. Section 12.8 reviews the theory of self-contained equilibria for a beam with current less than I_A in a resistive plasma. We shall study the Bennett equilibrium, a self-consistent model for magnetically-pinched beams with non-zero emittance. The Bennett equilibrium, based on a Maxwell distribution of transverse energy, is a good representation for collision-dominated beams. Section 12.9 applies the equilibrium results to model long-distance transport of an electron beam through a weakly-ionized plasma. Collisions with gas atoms increase the transverse emittance, resulting in an expanding beam envelope. We derive the Nordsieck length, an expression for the collision-limited propagation distance.

12.1. Space-charge neutralization in equilibrium plasmas

When a high-current beam enters a plasma, plasma particles move to cancel the beam-generated electric field. In this section we shall calculate the response of a plasma to a steady-state beam and investigate the significance of the plasma Debye length.

To begin we shall review the quantities we need to characterize a plasma. Plasmas are collections of ions and electrons governed by long-range electromagnetic interactions. Usually, the densities of ions and electrons, n_e and n_i, are almost equal so that the mixture is space-charge neutralized. In many experiments on plasma transport of electron beams the beam density n_b is much smaller than the plasma density, $n_b \ll n_e$. The beam drives out a few of the plasma electrons to achieve complete space-charge neutralization, where:

$$n_i = n_e + n_b. \tag{12.1}$$

Relativistic electron beams generate strong magnetic focusing forces. Such beams can be self-contained with only partial space-charge neutralization. Therefore, the transport of such beams in low-density plasmas ($n_b > n_e$) is of considerable interest. In this case the beam expels all the low-energy plasma electrons.

The kinetic energy of plasma particles affects how they respond to beams. In this chapter we shall represent the velocity dispersion of plasma ions and electrons as Maxwell distributions with

temperatures T_i and T_e. Plasma particles may also have average drift velocities $\mathbf{v}_i$ and $\mathbf{v}_e$. Usually unconfined plasmas are stable against velocity space instabilities if

$$|\mathbf{v}_i|, |\mathbf{v}_e| \ll (2kT_e/m_e)^{1/2}. \tag{12.2}$$

The condition of Eq. (12.2) holds when moderate-current beams propagate through dense plasmas. On the other hand, high-current pulsed electron beams can induce a large plasma electron drift velocity, leading to a two-stream instability and rapid plasma heating.

Plasmas used for electron beam transport usually have low temperature ($kT_e < 100$ eV), and large spatial extent. Methods for beam plasma generation include laser ionization, pulsed plasma guns, low-energy electron discharges or collisions of beam particles with a background gas. Beam-generated plasmas are often not fully ionized – neutral atoms are present in the beam volume. Although atoms do not participate in electromagnetic interactions, they may influence the beam and plasma responses through collisions.

We shall use a simple model to calculate the steady-state response of a plasma to an injected beam. The beam enters an unconfined plasma of infinite dimension with no included magnetic field. Low-energy electrons respond rapidly to the presence of the beam while the massive ions respond slowly. We neglect ion motion and assume that the beam pulse is long enough for plasma electrons to adjust to a modified equilibrium. The electron beam density is uniform in z and has cylindrical symmetry. We write the beam density as:

$$n_b(r) = n_{bo} f(r). \tag{12.3}$$

The function $f(r)$ equals unity on the axis and drops to zero on the beam envelope, $f(r_b) = 0$. The plasma ions are spatially uniform with density $n_i(r) = n_o$. If the electrons are in thermal equilibrium, their density is:

$$n_e(r) = n_o \exp(+e\phi(r)/kT_e). \tag{12.4}$$

The electrostatic potential $\phi(r)$ is negative over the region of interest. The form of Eq. (12.4) ensures that at large radius the potential drops to zero and the plasma electron density approaches the ion density.

Using Eqs. (12.3) and (12.4), the Poisson equation is:

$$\frac{1}{r}\frac{d}{dr}\left[r\frac{d\phi}{dr}\right] = \frac{e}{\epsilon_o}\left[n_{bo} f(r) - n_o + n_o \exp\left(\frac{e\phi}{kT_e}\right)\right]. \tag{12.5}$$

Equation (12.5) is similar to Eq. (11.44) for the neutralization of an ion beam by hot electrons. We again scale the potential in terms of kT_e and the length in terms of the Debye length [Eq. (6.13)]:

$$\Phi = -e\phi/kT_e, \tag{12.6}$$

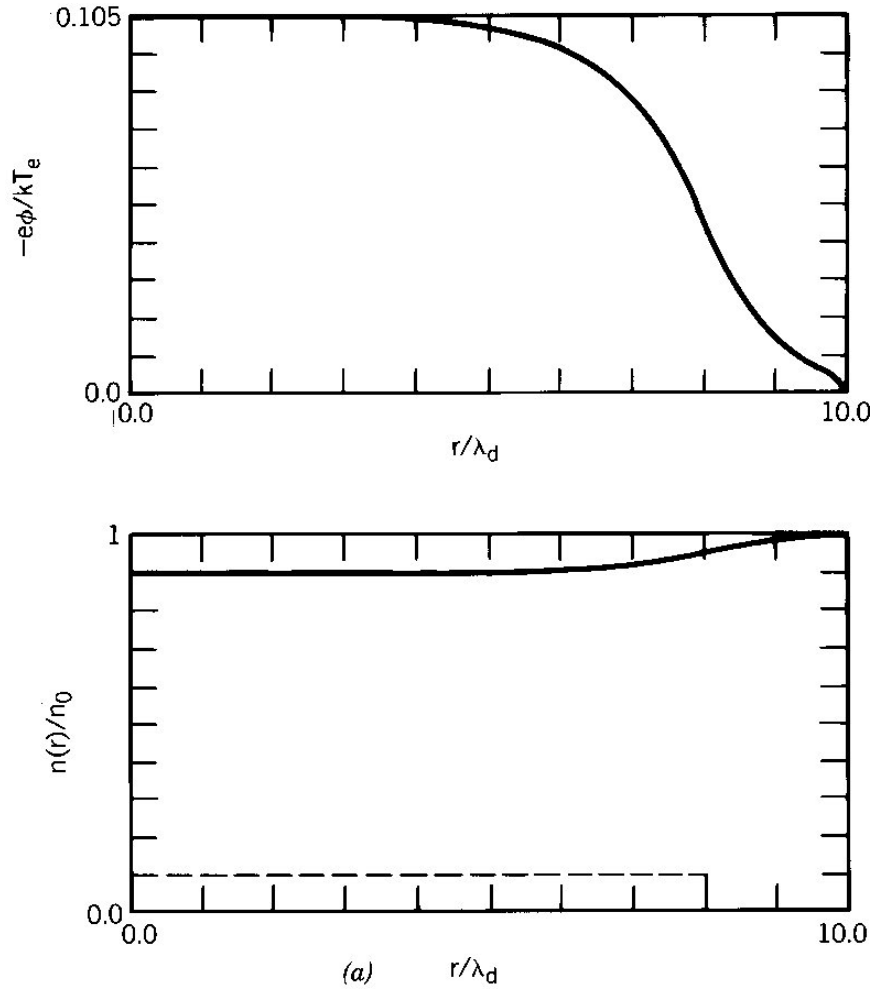

Figure 12.1.a. Neutralization of a steady-state, cylindrical electron beam in a homogeneous plasma. Numerical solutions for a broad beam. Unperturbed plasma electron density: n_o, plasma temperature: T_e, $\lambda_d = (kT_e\epsilon_o/e^2n_{eo})^{1/2}$. Beam has uniform density $n_{bo} = 0.1n_o$, and a sharp boundary at $r_b/\lambda_d = 8$. Top: spatial variation of electrostatic potential. Bottom: solid line, spatial variation of plasma electron density; dashed line, spatial variation of beam density.

$$R = r/\lambda_d. \tag{12.7}$$

The dimensionless form of Eq. 12.5 is

$$\frac{1}{R}\frac{d}{dR}\left[R\frac{d\Phi}{dR}\right] = -N_{bo}f(R) + [1 - \exp(-\Phi)], \tag{12.8}$$

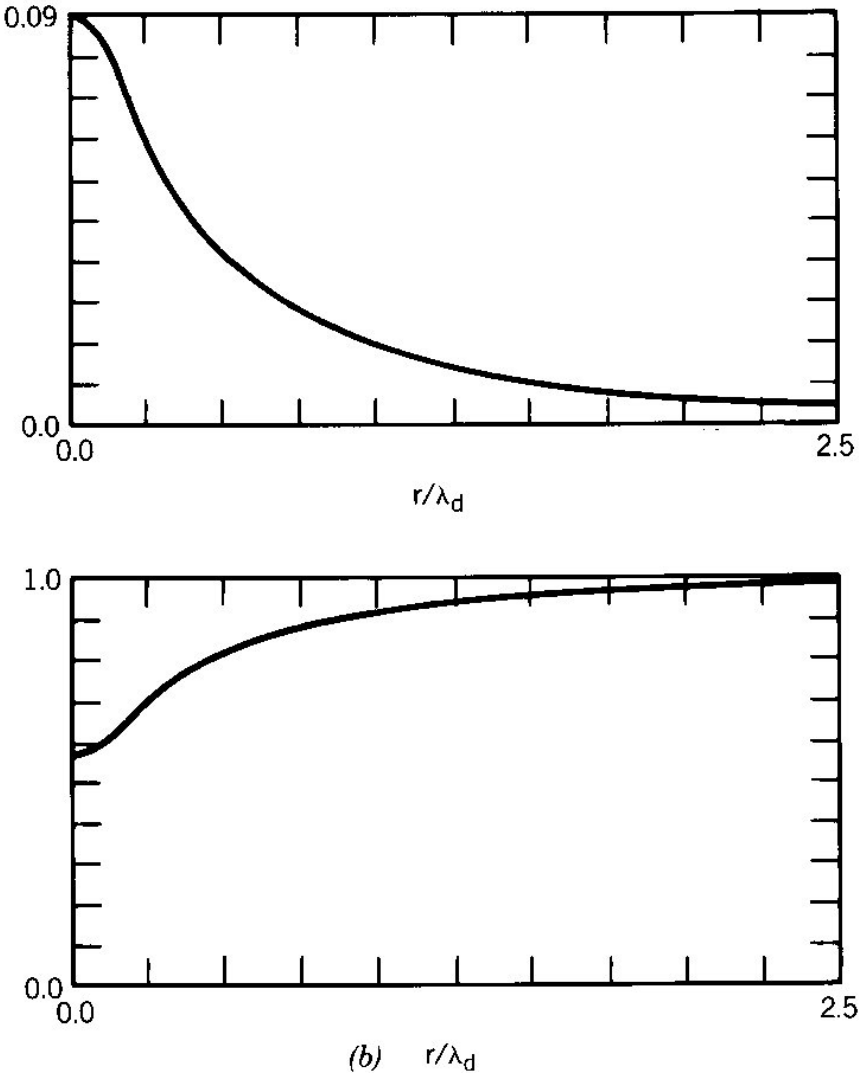

Figure 12.1.b. Analytic solution for Debye shielding of electric fields in a narrow beam, $r_b/\lambda_d \ll 8$. Top: Spatial variations of electrostatic potential. Bottom: Spatial variation of plasma electron density.

where $N_{bo} = n_{bo}/n_o$. Given $f(R)$ and a value for N_{bo}, we solve Eq. (12.8) by integrating from the origin with the symmetry condition $d\Phi/dR = 0$. The proper choice of $\Phi(0)$ gives a solution where $\Phi = 0$ and $d\Phi/dR = 0$ at large radius. This value of $\Phi(0)$ gives an electron density that preserves net neutrality:

$$\int_0^\infty 2\pi r dr\ n_e(r) = \int_0^\infty 2\pi r dr\ [n_o - n_b(r)]\ . \tag{12.9}$$

Figure 12.1*a* shows a solution of Eq. (12.8) for a broad beam ($r_b/\lambda_d = 8$) with a sharp boundary. The reduction of the plasma electron density equals the beam density over most of the beam width. Electric fields are concentrated within one Debye length of the beam edge. The on-axis potential energy $e\phi(0)$ is much smaller than kT_e if the beam density is low, $n_{bo} \ll n_o$.

The nature of Debye shielding in a plasma is often illustrated with the example of the fields of a point test particle with charge q. To find the distribution of plasma electrons, we solve the Poisson equation in spherical coordinates centered on the test particle. We assume that the test charge makes a small perturbation to the plasma distribution, or $q\phi(r)/kT_e \ll 1$. The approximate form of the Poisson equation is:

$$\frac{1}{r^2}\frac{d}{dr}\left[r^2\frac{d\phi}{dr}\right] \cong \frac{\phi}{\lambda_d^2} \; . \tag{12.10}$$

We solve Eq. (12.10) analytically with the boundary condition that the potential approaches the vacuum potential for a charge q as r approaches zero:

$$\phi(r) = (q/4\pi\epsilon_o r)\exp(-r/\lambda_d). \tag{12.11}$$

The expression of Eq. (12.11) is the product of the vacuum electrostatic potential times a term resulting from the plasma, $\exp(-r/\lambda_d)$. The plasma cancels the electric field of the test charge at distances greater than λ_d – the process is called *Debye shielding*. Figure 12.1*b* shows a numerical solution for a related case, an immersed narrow cylindrical electron beam with $r_b \ll \lambda_d$. The plasma shields the radial electric of the beam over a length scale equal to λ_d.

12.2. Oscillations of an un-magnetized plasma

To study the transport of pulsed beams we must understand time-dependent plasma processes. Section 12.4 presents numerical calculations of plasma response to a rapidly pulsed electron beam. As a preliminary, this section reviews analytic calculations of plasma oscillations induced by charge imbalances. We limit the discussion to uniform plasmas with infinite extent and no applied magnetic field. In this case all plasma disturbances oscillate at the plasma frequency, ω_{pe}. The quantity $1/\omega_{pe}$ is the characteristic time for plasma electrons to shift position to balance a charge perturbation.

Again, we shall make several approximations to simplify the mathematics and to emphasize the relevant physical processes:

1. The plasma oscillation is a small perturbation about a stationary state.

2. The motion of plasma particles is one-dimensional. Electric fields and particle displacements are in the x direction.

3. The plasma is cold, $kT_e = kT_i = 0$. As a result, the macroscopic electric force determines the motion of electrons. Because all electron orbits at a position x are identical, the first two moment equations (Section 2.10) gives a complete description.

4. Ions are immobile over time scales for electron motion.

5. Collisions have a negligible effect on electron dynamics. The time between collisions is much longer than $1/\omega_{pe}$.

The steady-state plasma has electron and ion densities that are uniform and equal:

$$n_{eo}(x) = n_{io}(x) = n_o. \tag{12.12}$$

Equation (12.12) implies that the equilibrium plasma has no electric field. The density of immobile ions remains uniform over time scales of interest:

$$n_i(x,t) = n_o. \tag{12.13}$$

We use moment equations to describe the electron response to a perturbation. The one-dimensional equation of continuity is:

$$\frac{\partial n_e}{\partial t} + \frac{\partial}{\partial x}(n_e v_e) = 0 \ . \tag{12.14}$$

The equation of momentum conservation for the non-relativistic plasma electrons is

$$\frac{\partial v_e}{\partial t} + v_e \frac{\partial v_e}{\partial x} = -\frac{eE}{m} \ . \tag{12.15}$$

The function E_x is the electric field resulting from displacement of the electrons. It is related to the electron density through the one-dimensional divergence equation:

$$\frac{\partial E_x}{\partial x} = \frac{e}{\epsilon} (n_o - n_e) \ . \tag{12.16}$$

The first term in parenthesis is the contribution of the uniform ion density.

Equations (12.14), (12.15) and (12.16) are a coupled set of non-linear differential equations. We can find an analytic solution in the limit of small changes from equilibrium. We write the variation of electron density as:

$$n_e(x,t) = n_o + \Delta n(x,t), \tag{12.17}$$

where $\Delta n \ll n_o$. In the equilibrium state, there is no average electron velocity or electric field. We denote the small perturbed values of these quantities as Δv and ΔE. The continuity equation becomes:

$$\frac{\partial \Delta n}{\partial t} + n_o \frac{\partial \Delta v}{\partial x} + \Delta n \frac{\partial \Delta v}{\partial x} = 0 \ . \tag{12.18}$$

We drop the third term in Eq. (12.18), a second-order differential quantity. Later, we shall prove that the term is small. The momentum equation takes the form:

$$\frac{\partial \Delta v}{\partial t} + \Delta v \frac{\partial \Delta v}{\partial x} = -\frac{e\Delta E}{m} \ . \tag{12.19}$$

We also eliminate the second term on the left-hand-side of Eq. (12.19). The divergence equation involves only the perturbed density:

$$\frac{\partial \Delta E}{\partial x} = -\frac{e\ \Delta n}{\epsilon_o} \ . \tag{12.20}$$

We can combine Eqs. (12.18), (12.19) and (12.20) into a single equation using the chain rule of partial derivatives:

$$\frac{\partial^2 \Delta n}{\partial t^2} = -\left[\frac{e^2 n_o}{m_e \epsilon_o}\right] \Delta n \ . \tag{12.21}$$

Equation (12.21) has the general solution

$$\Delta n(x,t) = f_1(x)\cos(\omega_{pe}t) + f_2(x)\sin(\omega_{pe}t). \tag{12.22}$$

The quantities $f_1(x)$ and $f_2(x)$ are arbitrary functions of position – they are constrained by the initial density and velocity variations in the plasma. For any initial state, the plasma response is oscillatory at the characteristic plasma frequency:

$$\omega_{pe} = \left[\frac{e^2 n_o}{m_e \epsilon_o}\right]^{1/2} . \tag{12.23}$$

The oscillation frequency of Eq. (12.23) is high for plasmas commonly used for electron transport. For example, a plasma with density 10^{19} m^{-3} has a plasma angular frequency of ω_{pe} =

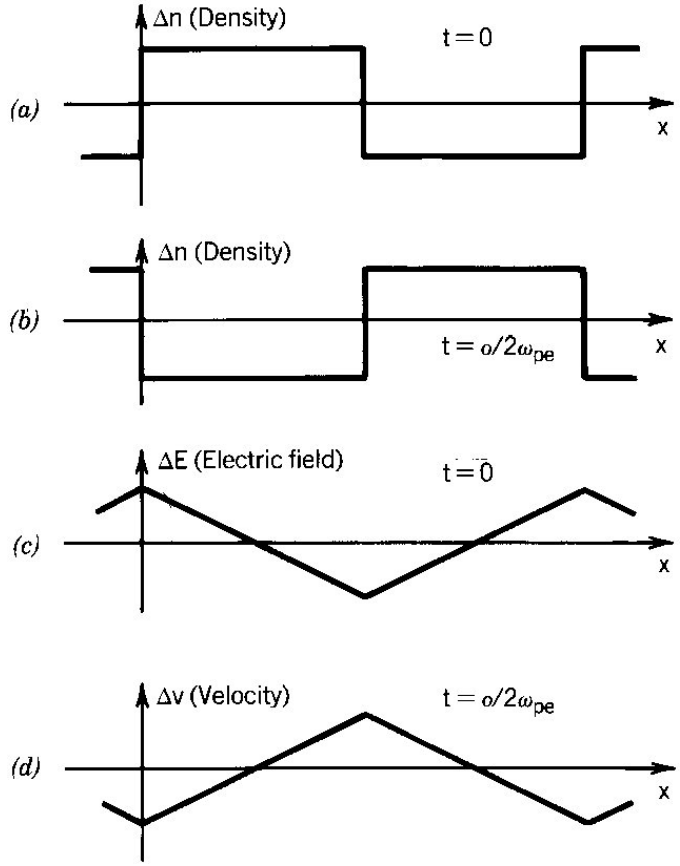

Figure 12.2. Mechanism of plasma oscillations. The initial perturbation of plasma electrons is a step function in density with no velocity change. *a*) Initial density perturbation. *b*) Density variation at $t = \pi/\omega_p$. *c*) Electric field distribution at $t = 0$. *d*) Velocity distribution at $t = \pi/2\omega_p$.

1.78×10^{11} s^{-1}. The oscillation frequency is $f = 28.4$ Ghz, corresponding to a period of only 0.035 ns.

To illustrate the physical meaning of Eq. (12.21), suppose we have a plasma with a specified initial density perturbation at $t = 0$ but with no initial electron velocity. Figure 12.2*a* illustrates the density perturbation, a step function that varies between $n_o \pm \Delta n_o$ over a spatial period of $2x_o$. For this special case, the function $f_1(x)$ is a step function and $f_2(x) = 0$. Equation (12.22) predicts that the density changes to the form shown in Figure 12.2*b* at $t = \pi/\omega_{pe}$. The regions with excess electron density become regions of minimum density. A plot of the electric field at $t = 0$ (Figure 12.2*c*) clarifies the mechanism of the density reversal. From Eq. (12.20) the initial electric field is a sawtooth function with maximum amplitude:

$$\Delta E = e\Delta n x_o/2\epsilon_o. \tag{12.24}$$

Equation (12.19) implies that the spatial variation of velocity is proportional to $-\Delta E(x)$ – the

temporal velocity variation is 90° out of phase with the electric field. Figure 12.2*d* illustrates the spatial variation of velocity at $t = \pi/2\omega_{pe}$. The direction of the velocity is such that electrons shift from regions of high density towards regions of low density. According to the equation of continuity, the linear spatial variation of velocity means that the density decreases uniformly over a region with $\Delta n > 0$.

We can use Eqs. (12.18) and (12.19) to estimate how far individual electrons move during the the density compression and rarefaction. The magnitudes of the perturbed position, velocity and electric field are related by

$$\Delta x = \Delta v/\omega_{pe} = e\Delta E/m_e\omega_{pe}^2 = x_o\,(\Delta n/n_o)/2. \tag{12.25}$$

In the limit that $\Delta n/n_o \ll 1$, the amplitude of individual particle oscillations Δx is much smaller than the length scale of the disturbance, x_o. Plasma oscillations result from small shifts of large numbers of electrons. We can use Eq. (12.25) to estimate the magnitudes of terms on the left-hand-side of Eq. (12.19). The time-derivative of a quantity is roughly equal to the magnitude of the quantity multiplied by ω_{pe} – a spatial derivative is comparable to the quantity multiplied by $1/x_o$. A dimensional analysis shows that the first term of Eq. (12.19_ has magnitude:

$$\partial\Delta\underline{v}/\partial\underline{t} \le \omega_{pe}\Delta v, \tag{12.26}$$

while the second term is

$$\Delta v(\partial\Delta v/\partial x) \le \Delta v^2/x_o \cong (2\Delta v^2/\Delta x)(\Delta n/n_o) \cong (\omega_{pe}\Delta v)\,(\Delta n/n_o). \tag{12.27}$$

The non-linear term is smaller by a factor of $(\Delta n/n_o)$. Hence, we were justified dropping it from the analysis.

The plasma oscillations represented in Figure 12.2 are stationary. We can generate traveling wave oscillations if the initial electron distribution includes perturbations in both density and velocity. Because Eqs. (12.18), (12.19) and (12.20) are linear, we can represent any initial variation and subsequent oscillation as a sum of independent harmonic components. Suppose that the density perturbation at t = 0 has the form:

$$\Delta n(x,0) = \Delta n_o \cos(kx) \tag{12.28}$$

and the initial velocity variation equals:

$$\Delta v(x,0) = -\frac{\omega_p}{k}\,\frac{\Delta n_o}{n_o}\,\cos(kx)\ . \tag{12.29}$$

Equations (12.28) and (12.29) imply that the spatial functions of Eq. (12.22) are:

$$f_1(x) = \cos(kx), \tag{12.30}$$

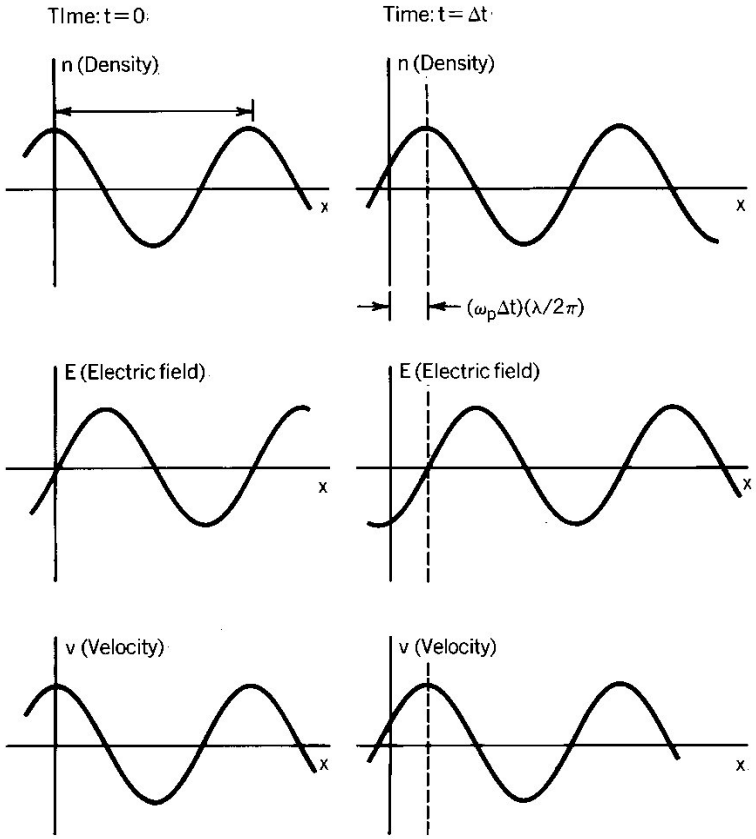

Figure 12.3. Relationships between perturbed electron density, velocity, and electric field for a plasma wave with a positive phase velocity. Left-hand-side: t = 0, right-hand-side: $t = \Delta t$.

and

$$f_2(x) = \sin(kx).$$

Combining the trigonometric terms of Eq. (12.22), we can express the density as:

$$\Delta n(x,t) = \Delta n_o \cos(kx - \omega_{pe} t). \tag{12.31}$$

Equation (12.31) is a traveling density perturbation with phase velocity ω_{pe}/k. Such waves are called *plasma waves*. Plasma waves oscillate at frequency ω_{pe}. They may have any phase velocity, depending on the choice of wave number. As an example, suppose we inject a 100 keV electron beam into a plasma with density $n_o = 10^{19}$ m^{-3}. The electron beam interacts strongly with plasma waves if the phase velocity of the wave equals the beam velocity, $v_z = \beta c$, where $\beta = 0.548$. Here, beam electrons move with a point of constant phase and see a steady state electric field. The condition for resonant interaction is

$$\omega/k = \beta c, \tag{12.32}$$

or

$$\lambda = 2\pi\beta c/\omega_{pe}.$$

For the given plasma density, we expect to observe the growth of plasma waves with $\lambda \cong 5.8 \times 10^{-3}$ m.

For a harmonic disturbance moving in the $+x$ direction, the density, velocity and electric field are given by

$$\Delta n(x,t) = \Delta n_o \cos(kx-\omega_{pe}t). \tag{12.33}$$

$$\Delta E = \frac{e\Delta n_o}{\epsilon_o k} \sin(kx-\omega_{p_e}t) . \tag{12.34}$$

and

$$\Delta v = \frac{\Delta n_o}{n_o} \frac{\omega_{pe}}{k} \cos(kx-\omega_{pe}t) . \tag{12.35}$$

Figure 12.3 illustrates the relations between plasma quantities in the moving disturbance. The left-hand-side of the figure shows the initial plasma state while the right-hand-side shows the quantities after an interval Δt. First, consider the velocity variation. In the region between $x = 0$ and $x = \lambda/2$, the velocity decreases as x increases. Therefore, in this region the velocity dispersion bunches particles (Section 15.3) and the density increases. Conversely, electrons disperse in the region $-\lambda/2 \le x \le 0$ so that the density decreases. The combination of increasing and decreasing density causes the point of maximum density to move to the right. Inspection of the spatial variation of electric field shows that electrons accelerate in the region $0 \le x \le \lambda/2$ and decelerate at position $-\lambda/2 \le x \le 0$. The combination of increasing and decreasing velocity causes the point of maximum velocity to move to the right.

12.3 Oscillations of a neutralized electron beam

In this section, we shall show that a uniform current-density electron beam in a neutralizing ion background oscillates at a characteristic frequency. The beam oscillation frequency is called the *beam plasma frequency* because it has the same form as the plasma frequency of Section 12.2. We shall apply the results in Sect. 13.6 to study hose instabilities of ion-confined electron beams.

We shall begin by modeling a non-relativistic electron beam and add relativistic corrections

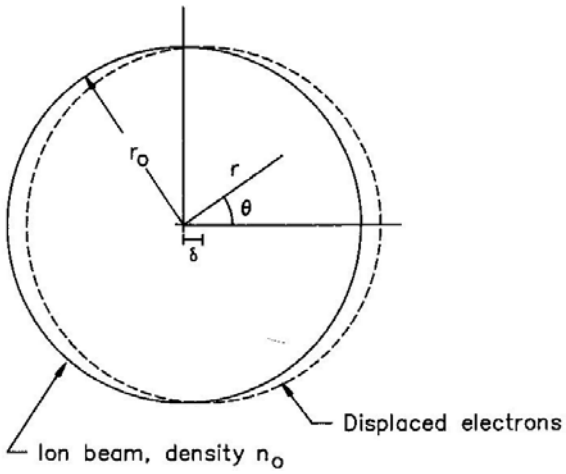

Figure 12.4. Coordinates to analyze transverse oscillations of a cylindrical non-relativistic electron beam in an ion background.

later. A cylindrical electron beam with uniform density n_e from the axis to radius r_o moves through an equal density of ions, $n_i = n_e = n_o$. The massive ions are immobile in the transverse direction. In equilibrium, there is no electric field. Electrons move in the axial direction with velocity v_z. For $v_z/c \ll 1$, the effect of beam-generated magnetic forces is small. We shall calculate the response of the beam to a perturbation in the electron rest frame moving at velocity v_z. The condition $v_z \ll c$ means that the particle densities and electric fields are almost the same in the rest frame and laboratory frame.

Suppose that at $t = 0$ we displace all electrons a distance $\delta(z,0)$ from the ions (Figure 12.4). The charge separations results in an electric field E_x. The electrons subsequently oscillate about the immobile ion core. The quantity $\delta(z,t)$ represents the time-dependent displacement of the beam center. We can calculate the nature of beam oscillations with the following assumptions:

1. The displacement is small, $\delta \ll r_o$.

2. The electrostatic approximation is valid for the calculation of fields – electromagnetic radiation from the beam is negligible.

3. The axial length for variations of the displacement is much greater than r_o.

The second conditions holds if the oscillation period is much longer than r_o/c. With the third assumption, we can approximate local fields with expressions for an infinite length beam.

As a first step, we shall find the electric field that results from a uniform electron displacement using the polar coordinate system of Figure 12.4. The figure shows the effect of a small electron beam displacement. Although the core of the beam maintains zero charge density, there is a charge imbalance on the surface. For small displacement, we can represent the charge as a thin

surface layer. The magnitude of the surface charge density is proportional to the thickness of the layer – Figure 12.4 shows that

$$\sigma \text{ (coulombs/m}^2) = -en_o\sigma\delta \cos\theta. \tag{12.36}$$

Gauss' law implies that the electric fields inside and outside the beam surface are related by:

$$E_\theta(\text{out}) = E_\theta(\text{in}), \tag{12.37}$$

$$E_r(\text{out}) = E_r(\text{in}) + \sigma/\epsilon_o. \tag{12.38}$$

To find the electric field, we can solve the Laplace equation for electrostatic potential inside and outside the surface and match the values of the potential at $r = r_o$ using Eqs. (12.37) and (12.38). The Laplace equation is valid within the beam core because there is no net space-charge.

For an axially uniform system, the Laplace equation is:

$$\frac{1}{r}\frac{d}{dr}\left[r\frac{d\phi(r,\theta)}{dr}\right] + \frac{1}{r^2}\frac{d^2\phi(r,\theta)}{d\theta} = 0. \tag{12.39}$$

The method of separation of variables gives a general solution for Eq. (12.39). We take the potential as:

$$\phi(r,\theta) = R(r)\Theta(\theta). \tag{12.40}$$

Substitution of Eq. (12.40) into Eq. (12.39) gives individual equations for the radial and azimuthal functions $R(r)$ and $\Theta(\theta)$. We can write the general solution in terms of cylindrical harmonic functions:

$$\phi(r,\theta) = \sum_{n=0}^{\infty} R_n(r)\,\Theta_n(\theta)\ . \tag{12.41}$$

where

$$\Theta_o = A_o\theta + B_o, \tag{12.42}$$

$$R_o = C_o \ln r + D_o, \tag{12.43}$$

$$\Theta_n = A_n \cos(n\theta) + B_n \sin(n\theta), \tag{12.44}$$

and

$$R_n = C_n r^n + D_n r^{-n}. \tag{12.45}$$

The electrostatic potential for the geometry of Figure 12.4 must have symmetry about the y axis;

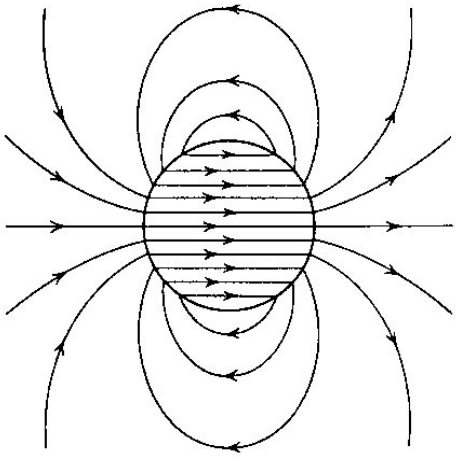

Figure 12.5. Electric field lines resulting from small upward displacement of a cylindrical electron beam in an ion background (Adapted from J.D. Jackson, **Classical Electrodynamics**. Used by permission, John Wiley and Sons).

therefore, we can drop the sine terms in the expansion of Eq. (12.44). The requirement that the potential inside the beam has a finite value at the origin reduces the expansion to the following form:

$$\phi_{in}(r,\theta) = \sum_{n=1}^{\infty} M_n \, r^n \cos(n\theta) \; . \tag{12.46}$$

Similarly, the potential in the region $r > r_o$ approaches zero at large radius. Here, the potential is:

$$\phi_{out}(r,\theta) = \sum_{n=1}^{\infty} N_n \, r^{-n} \cos(n\theta) \; . \tag{12.47}$$

We can determine the coefficients in Eqs. (12.46) and (12.47) by matching the solutions at $r = r_o$. Note that the equations must hold at all values of θ. Therefore all coefficients except those with $n = 1$ equal zero. The constraints on the coefficients for $n = 1$ imply that the electrostatic potential is:

$$\phi_{out}(r,\theta) = (\sigma r_o^2/\epsilon_o)\,(\cos\theta/r), \tag{12.48}$$

$$\phi_{in}(r,\theta) = (\sigma/\epsilon_o)\, r\cos\theta \; = (\sigma/\epsilon_o)\, x. \tag{12.49}$$

Figure 12.5 plots electric field lines for the potential of Eqs. (12.48) and (12.49). Outside the beam, the potential is identical to that of an electric dipole located at the origin.

The implication of Eq. (12.49) is that the x directed electric field inside the beam volume is constant,

$$E_x = -en_o\,\delta/\epsilon_o. \tag{12.50}$$

A uniform displacement of electrons gives a uniform electric field. The equation of motion for all electrons inside the beam core is

$$m_e\,(d^2\delta/dt^2) = -(e^2 n_o/\epsilon_o)\,\delta. \tag{12.51}$$

Equation (12.51) implies that in the beam rest frame the electrons oscillate at frequency $\omega_{pe} = (e^2 n_o/\epsilon_o m_e)^{1/2}$. We can write the transverse beam motion of the beam in the general form:

$$\delta(z,t) = \delta(z)\ \mathrm{Re}\ \exp[\omega_{pe}t + \phi(z)]. \tag{12.52}$$

The quantities $\delta(z)$ and $\phi(z)$ are arbitrary amplitude and phase factors that depend on the initial perturbation. As with any collection of independent oscillators, we can construct standing wave or traveling wave disturbances by choosing appropriate forms of $\phi(z)$. With $\delta(z)$ uniform and $\phi(z) = \pm kz$, Eq. (12.52) represents a traveling wave with phase velocity $\pm\omega/k$.

Neutralized relativistic electron beams also can perform transverse electrostatic oscillations. To develop a theory for this regime, we assume that the change of energy in the transverse direction is much smaller than the electron kinetic energy $(\gamma\text{-}1)m_o c^2$. A uniform cylindrical beam of electrons of density n_b travels through a uniform ion cylinder with equal density n_i. In the laboratory frame there is a beam-generated magnetic force. This force is always symmetric about the center of the beam so it does not contribute to transverse oscillations. The asymmetric charge distribution of the displaced beam acts like a surface charge layer:

$$\sigma = -en_b\,\sigma\delta\,\cos\theta. \tag{12.53}$$

Following the previous discussion, the charge layer creates a uniform electric field $E_x = -en_b\,\delta/\epsilon_o$. To calculate the electron response to the field, we must remember that they have relativistic mass γm_o in the laboratory frame. The electron beam oscillates at ω_b, the *beam plasma frequency*:

$$\omega_b = \left[\frac{n_b e^2}{\gamma m_o \epsilon_o}\right]^{1/2}. \tag{12.54}$$

The beam oscillation frequency differs from Eq. (12.54) if the beam and ion densities are unequal. Generally n_b is greater than n_i for a neutralized relativistic electron beam in equilibrium. For example, Section 5.5 showed that a uniform-density electron beam with zero emittance in a uniform ion background of the same radius has radial force balance when

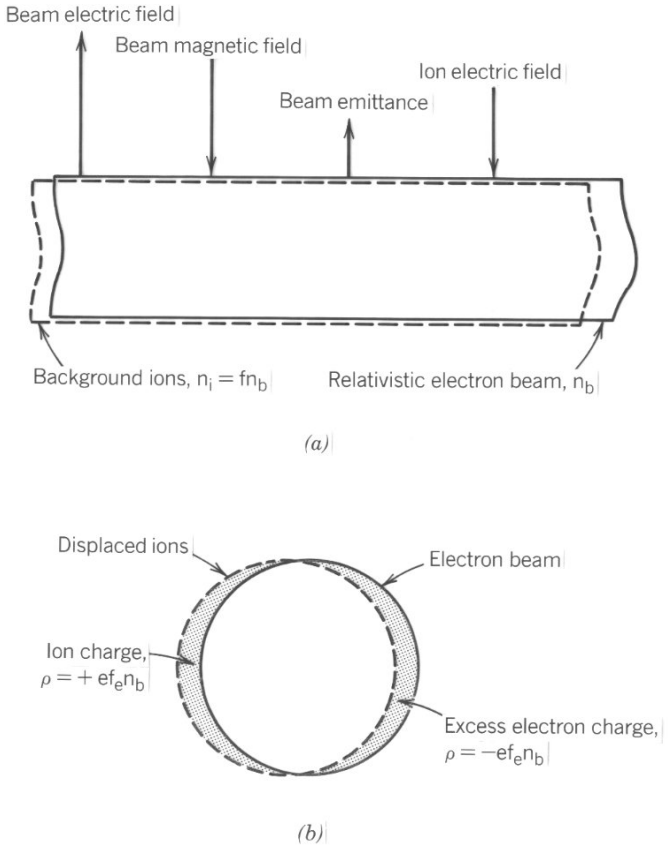

Figure 12.6. Partial neutralization of a relativistic electron beam by an ion background. *a*) Radial forces acting on the beam in equilibrium. *b*) Charge distribution for a displaced beam.

$$n_i = n_b/\gamma^2. \tag{12.55}$$

The ions cancel only a fraction of the radial electric field. The ion density for equilibrium must be higher if the electron beam has non-zero emittance. We can symbolize the relation between ion and beam densities by the neutralization fraction [Eq.)5.124)]:

$$f_e = n_i/n_b,$$

where $f_e \geq 1/\gamma^2$.

Suppose an electron beam moves through an ion background of density $f_e n_b$. Figure 12.6*a* illustrates forces on an equilibrium electron beam in the laboratory frame. With no displacement, there is a balance between the forces of the net radial electric field, emittance, and the beam-generated magnetic field. Figure 12.6*b* shows forces when the beam moves sideways a small distance δ. The beam-generated magnetic force and the emittance force are unaffected by the displacement. To calculate the electric force, we divide the beam charge into two components

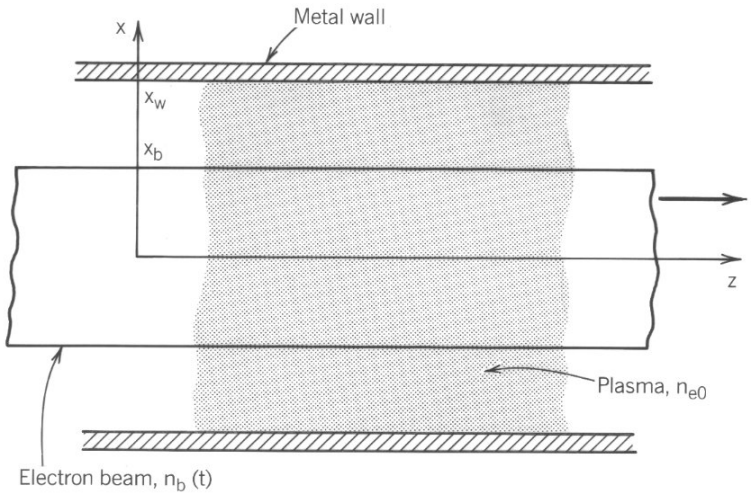

Figure 12.7. Geometry for numerical solutions of fluid equations describing the injection of a pulsed electron into a homogeneous, field-free plasma.

with densities $(1\text{-}f_e)n_b$ and $f_e n_b$. The first component creates a radial electric field centered on the beam axis with magnitude equal to the magnetic and emittance forces – it does not contribute to transverse beam oscillation. The second component, when combined with the displaced ion charge, approximates the effect of a charge layer $\sigma = -e(f_e n_b)\sigma\delta\cos\theta$. The result is that the beam oscillates at frequency

$$\omega_\perp = \left[\frac{f_e\, n_b\, e^2}{\gamma m_o \epsilon_o}\right]^{1/2}. \qquad (12.56)$$

12.4. Injection of a pulsed electron beam into a plasma

In this section, we shall study detailed solutions for the response of a plasma to a rapidly pulsed electron beam using the moment equations of Section 2.10. The model illustrates the excitation of plasma oscillations by a pulsed beam. It also gives us another opportunity to apply numerical methods to the solution of collective problems. We shall solve a set of non-linear moment equations using the Lax-Wendroff method.

In collective problems the preliminary analysis and simplifying assumptions are as important as the actual solution. To describe plasma neutralization of a pulsed beam, we want to reduce the problem so that the solutions have generality and do not depend critically on details of the boundary conditions. Nonetheless we must be certain to include the essential physical processes so that the results reflect the behavior of real systems. Figure 12.7 illustrates the geometry of the calculation. A sheet beam of high-energy electrons enters a uniform, fully-ionized plasma

enclosed between conducting boundaries at $\pm x_w$. The plasma has an equilibrium electron density of n_{eo}. The beam has half-width x_o.

To reduce the mathematical complexity, we limit attention to solutions where all quantities vary only in the x direction. This assumption is not entirely consistent – the density of a pulsed beam must change along the direction of propagation. In particular if the beam current at a position on the z axis has risetime Δt_b, then the density varies over the axial length $v_z \Delta t_b$. A one-dimensional calculation gives a good prediction of the local behavior of the plasma if

$$x_w \ll v_z \Delta t_b. \tag{12.57}$$

We shall adopt the condition of Eq. (12.57) and ignore z derivatives. In the local region of the calculation, the beam density varies with time. We take the beam density as uniform between $\pm x_o$ with a time variation:

$$n_b(t) = n_{bo}\, g(t). \tag{12.58}$$

The function $g(t)$ varies from 0 to 1 over the beam rise time Δt_b.

To simplify the model further, we assume that there are no applied magnetic fields and that the beam-generated magnetic fields are small. The calculation of electric fields is easy if we neglect electromagnetic radiation. The electrostatic limit applies if the relaxation time of the plasma is much longer than the time for electromagnetic radiation to cross the system:

$$1/\omega_{pe} \gg x_w/c. \tag{12.59}$$

Finally we use the approximation of immobile plasma ions – the ion density equals n_{eo} over the duration of the calculation. The validity condition is:

$$1/\omega_{pi} \gg \Delta t_b. \tag{12.60}$$

In Eq. (12.60) ω_{pi} is the ion plasma frequency:

$$\omega_{pi} = \left[\frac{e^2\, n_{eo}}{m_i\, \epsilon_o}\right]^{1/2}. \tag{12.61}$$

The quantity $1/\omega_{pi}$ is the time for ions to respond to an imbalance of space-charge.

With a stiff beam and immobile ions we need solve only moment equations for plasma electrons. We take the plasma electrons as cold. The effects of electron temperature are small if $kT_e \ll e|\phi|$, where $|\phi|$ is the magnitude of electrostatic potential created by the injection of the beam. In the cold-electron limit we can describe the plasma completely with the Poisson equations and the equations of continuity and momentum conservation (Section 12.10). We can write the coupled set of equations in a convenient form by defining dimensionless variables. The

dimensionless plasma electron density is referenced to the equilibrium density before injection of the beam:

$$N = n_e/n_{eo}. \tag{12.62}$$

Similarly, the dimensionless maximum beam density is $N_{bo} = n_{bo}/n_{eo}$. As we saw in Section 12.2, there is no inherent length scale associated with plasma oscillations. Therefore we choose a length scale characteristic of the specific problem, x_w. The dimensionless distance is

$$X = x/x_w. \tag{12.63}$$

The space-charge imbalance created by the beam induces a plasma oscillation. The characteristic time scale is $1/\omega_{pe}$ – dimensionless time is

$$\tau = \omega_{pe}\, t. \tag{12.64}$$

We normalize the velocity in terms the maximum velocity of plasma waves in the system:

$$V = v_e/(x_w\, \omega_{pe}). \tag{12.65}$$

Finally, we scale the electric field E_x in terms of the maximum field that results if bare plasma electrons fill the entire region between the conducting boundaries. The dimensionless electric field is

$$\mathbf{E} = E_x/(-en_{eo}\, x_w/\epsilon_o). \tag{12.66}$$

Recasting a numerical calculation in dimensionless variables is a valuable procedure because the quantities have magnitudes than we can compare to unity. This makes it easier to choose reasonable input parameters, to recognize errors, and to interpret results. For example, an effective plasma neutralization solution has $\mathbf{E} \ll 1$. Inserting the dimensionless variables, the equation of continuity [Eq. (2.102)] becomes:

$$\frac{\partial N}{\partial \tau} = -N\,\frac{\partial V}{\partial X} - V\,\frac{\partial N}{\partial X}\,. \tag{12.67}$$

The equation of momentum conservation is:

$$\frac{\partial V}{\partial \tau} = -\frac{1}{2}\frac{\partial}{\partial X}\,(V^2) - \mathbf{E}\,. \tag{12.68}$$

The first term on right-hand-side of Eq. (12.68) represents a change of momentum at a point by electron convection. The second term is the momentum change resulting from space-charge

electric fields. The dimensionless form of the Poisson equation is:

$$\frac{\partial \mathbf{E}}{\partial X} = 1 - N - N_{bo}\, g(\tau) \ . \tag{12.69}$$

For a solution on a digital computer, we must convert continuous differential equations to a discrete form. The usual approach is to define approximations to the continuous quantities at a finite set of locations, replacing the spatial and temporal derivatives in the original equations with finite-difference operators. For the present problem we define the quantities N, V and $\mathbf{E}$ at *NMesh* locations separated by a uniform distance ΔX. To calculate the evolution of the quantities in time, we advance them through a large number of states separated by a uniform interval $\Delta\tau$. Figure 12.8*a* shows quantities used in the discrete formulation. The set of discrete positions and times is called a *numerical mesh* or *grid*. We specify spatial position with the index j and temporal position by the index n. Discrete quantities defined at *mesh points* represent the original continuous functions:

$$N(X,\tau) \triangleright N(j,n). \tag{12.70}$$

The difference equations that advance $N(j,n)$, $V(j,n)$ and $\mathbf{E}(j,n)$ are correct if the discrete quantities approach the values of the continuous quantities at all positions and times in the limit that ΔX, $\Delta\tau \triangleright 0$.

We must define the mesh parameters clearly. Mesh quantities along the time axis are simple – time starts at zero and proceeds continuously until the end of the calculation. If we take $n = 0, 1, 2,...$then $\tau = n\Delta\tau$. The spatial mesh has boundaries. If the spatial index has the range $j = 0, 1, 2,...,$*NMesh*-1, *NMesh*, then the spatial position is

$$X = j\,\Delta X. \tag{12.71}$$

In the present problem, the final mesh point corresponds to the conducting wall at $X = 1$; therefore, the mesh spacing is $\Delta X = 1/$*NMesh*.

The two primary concerns of computer calculations are to preserve numerical stability and to achieve good accuracy. We shall discuss the stability criterion later. Regarding accuracy, we want results that are in close agreement with an exact solution of the partial differential equations. A necessary condition for a valid solution is that the quantities ΔX and $\Delta\tau$ must be smaller than the finest spatial or temporal features of the problem. For example, we want the time-step to be smaller than $1/\omega_{pe}$ – in our dimensionless units, this is equivalent to $\Delta\tau < 1$. We also want the total computational time to be as short as possible; therefore, $\Delta\tau$ should not be too small. The best approach is to choose a numerical method that gives good accuracy for a moderate number of computational steps. Here we shall review the two-step Lax-Wendroff method. The errors that result from this finite-difference formulation are on the order of ΔX^2 or $\Delta\tau^2$; therefore, the numerical solutions converge rapidly toward the exact solution as the step size decreases.

The Lax-Wendroff method [see, for instance, D. Potter, **Computational Physics** (Wiley, New

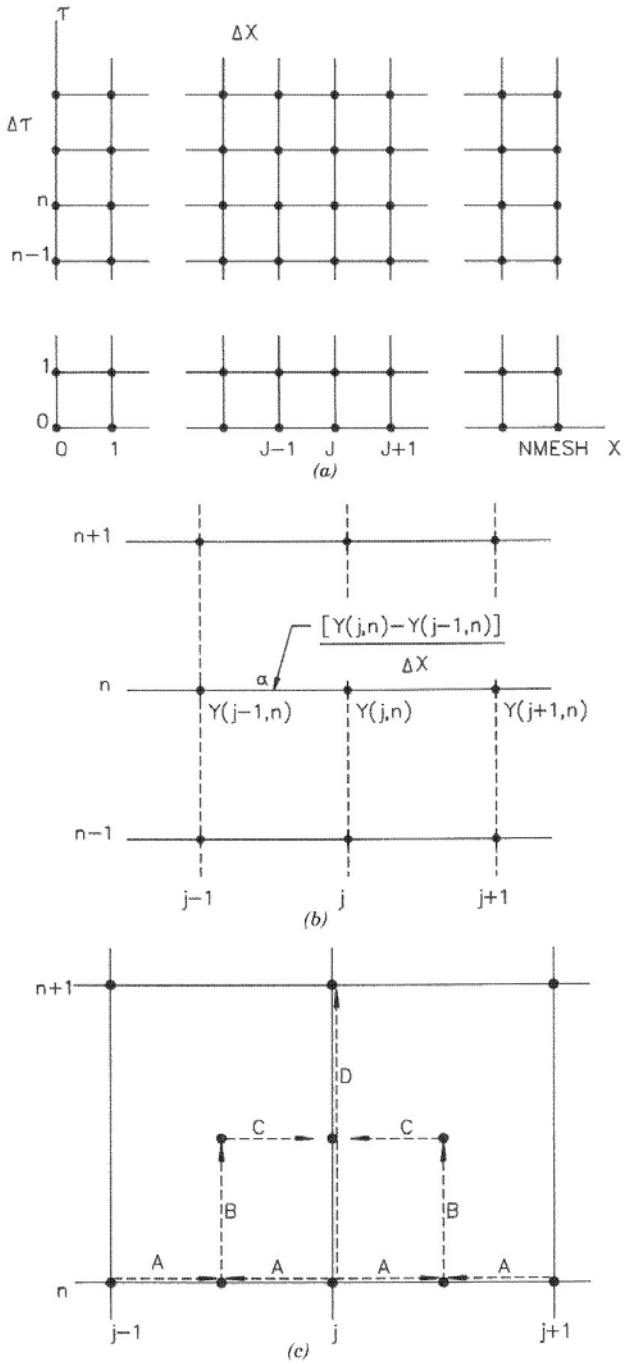

Figure 12.8. Elements of the finite-difference solution of fluid equations. *a*) Definition of a computational mesh in time and a single spatial dimension. Conventions for indices. *b*) Approximation for the spatial derivative of Y at position $j\Delta\chi$ and time $n\Delta\tau$. *c*) Strategy of the Lax-Wendorf method for a time- and space-centered solution of the convective fluid equation.

York, 1973), p. 67] is effective for partial differential equations like Eqs. (12.67) and (12.68) where the time derivatives are proportional to the spatial derivations. Section 2.3 stressed the importance of time-centering for ordinary differential equations. In this section we shall extend the two-step method to partial differential equations and seek equations centered in both space and time. Before attacking the coupled non-linear moment equations, we shall illustrate the method with the simple equation:

$$\partial Y(X,\tau)/\partial\tau = -\,\partial Y(X,\tau)/\partial X. \tag{12.72}$$

Figure 12.8*b* shows the strategy of the numerical solution. Suppose we have a discrete set of values of Y defined over the spatial mesh at time $\tau = n\Delta\tau$. We denote these values as $Y(j,n)$. The object is to advance the values to the next time step, generating a set $Y(j,n+1)$ that agrees with Eq. (12.72). The finite difference approximation for the spatial derivative of Y at time n is:

$$\partial Y(j+\tfrac{1}{2},n)/\partial X \cong [Y(j+1,n) - Y(j,n)]/\Delta X. \tag{12.73}$$

Note that the derivative is referenced to a location between two mesh points at time n (point α in Figure 12.8*b*). Following the discussion of time centering in Section 2.3, an accurate way to advance Y with Eq. (12.72) is to use the spatial derivative at a spatial mesh point and at a time $n+\tfrac{1}{2}$ (point β in Figure 12.8*b*):

$$Y(j,n+1) - Y(j,n) - [\partial Y(j,n+\tfrac{1}{2})/\partial X]\Delta\tau. \tag{12.74}$$

We can estimate the derivative at the intermediate time point by the two-step process shown schematically in Figure 12.8*c*:

In the first step, we calculate quantities at intermediate space and time steps from Eq. (12.72):

$$Y(j+\tfrac{1}{2}, n+\tfrac{1}{2}) = [Y(j+\tfrac{1}{2}, n) + Y(j, n)]/2 - \{[Y(j+\tfrac{1}{2}, n) - Y(j, n)]/\Delta X\}\,\{\Delta\tau/2\}. \tag{12.75}$$

The first term on the right hand side of Eq. (12.75) is the average value of Y at time n between spatial mesh points j and $j+1$. The second term is the change in Y in the interval $\Delta\tau/2$ using the spatial derivative at the point $(j+\tfrac{1}{2}, n)$. Next, we can use the values $Y(j+\tfrac{1}{2}, n+\tfrac{1}{2})$ to estimate the derivative at a time-centered position, $\partial Y(j, n+\tfrac{1}{2})/\partial X$. We then apply the derivatives to advance the set of $Y(j,n)$:

$$Y(j,n+1) = Y(j,n) - [Y(j+\tfrac{1}{2},n+\tfrac{1}{2}) - Y(j-\tfrac{1}{2},n+\tfrac{1}{2})](\Delta\tau/\Delta X). \tag{12.76}$$

Note that second term on the right-hand side approximately equals the desired time-centered derivative of Eq. (12.74).

To show how to apply the algorithm to a real problem, we shall write out all terms to advance the set of non-linear equations for plasma neutralization [Eqs. (12.67), (12.68) and (12.69)]:

First Step

A. Continuity equation

The expression to find intermediate values of the density from the continuity equation is straightforward:

$$N(j+½,n+½) = [N(j+1,n)+N(j,n)]/2 \qquad (12.77)$$

$$- (\Delta\tau/2)\,[N(j+1,n)+N(j,n)]/2\,[V(j+1,n)-V(j,n)]/\Delta X$$

$$- (\Delta\tau/2)\,[V(j+1,n)+V(j,n)]/2\,[N(j+1,n)-N(j,n)]/\Delta X.$$

B. Momentum equation

The momentum equation is more involved - we need values of the electric field at intermediate spatial points, $E(j+½,n)$. Following Eq. (12.69), we can evaluate the electric field by an iterative numerical integration:

$$E(½,n) = [1 - N_{bo}g(n) - N(0,n)](\Delta X/2), \qquad (12.78)$$

$$E(j+½,n) = E(j-½,n) + [1 - N_{bo}g(n) - N(j,n)](\Delta X/2).$$

Using the shifted electric field values, the first step to advance the momentum equation is:

$$V(j+½,n+½) = [V(j+1,n) + V(j,n)]/2 - (\Delta\tau/2)\,E(j+½,n) - (\Delta\tau/2)\,[V(j+1,n)^2 - V(j,n)^2]/(2\Delta X). \qquad (12.79)$$

Second Step

With the intermediate quantities $N(j+½,n+½)$ and $V(j+½,n+½)$ we proceed to the second step. Again we need to calculate electric field – this time at the time centered mesh position:

$$E(0,n+½) = 0, \qquad (12.80)$$

$$E(j,n+½) = E(j-1,n+½) + [1 - N_{bo}g(n) - N(j-½,n+½)](\Delta X/2).$$

The equations to advance N and V through a full time step are:

$$N(j,n+1) = N(j,n) \qquad (12.81)$$

$$- \Delta\tau\,\{[N(j+½,n+½)+N(j-½,n+½)]/2\}\,\{[V(j+½,n+½)-V(j-½,n+½)]/\Delta X\}$$

$$- \Delta\tau\,\{[V(j+½,n+½)+V(j-½,n+½)]/2\}\,\{[N(j+½,n+½)-N(j-½,n+½)]/\Delta X\}$$

and

$$V(j,n+1) = V(j,n) - \Delta\tau\, \mathrm{E}(j,n+\tfrac{1}{2}) - \Delta\tau\, [V(j+\tfrac{1}{2},n+\tfrac{1}{2})^2 - V(j-\tfrac{1}{2},n+\tfrac{1}{2})^2]/(2\Delta X). \qquad (12.82)$$

In the plasma neutralization problem we must include boundary conditions at the extremities of the mesh, $j = 0$ and $j = NMesh$. The problem has symmetry about $X = 0$. We can carry out the solution in the upper half x plane with the conditions:

$$\mathrm{E}(0) = 0, \quad V(0) = 0, \quad \partial N(0)/\partial X = 0. \qquad (12.83)$$

The boundary conditions at the conducting wall are more subtle. We must assign spatial derivatives of quantities at the wall that are consistent with physical processes in the plasma. One way to define a derivative at $j = NMesh$ is to add a virtual mesh point within the conducting wall at $j = NMesh+1$. We can think of the wall as a grounded zero-thickness foil – plasma electrons can stream out through the foil. Within the wall space-charge electric fields are completely canceled. Because there are no forces on electrons inside the wall there is no difference in the velocity between the last two points, $V(NMesh,n) = V(NMesh+1,n)$ – the derivative at the intermediate point always equals zero. Similarly the continuity equation implies that the electron density at the two points is the same, $N(NMesh) = N(NMesh+1)$. Note that electrons at the virtual mesh point have no effect on electric fields in the plasma. The virtual mesh point resolves some mathematical difficulties but has little effect on the physical results.

We must add other constraints at the wall to represent absorption of the plasma electrons. Because electrons cannot flow inward from the wall the value of V at $j = NMesh$ cannot be negative. Therefore, whenever the density and velocity values in adjacent cells imply a negative value of $V(NMesh,n)$, we set the quantity equal to zero. We also set $N(Nmesh)$ equal to zero because the wall cannot supply electrons to compensate for electron flow to inner cells.

Table 12.1 lists the body of a computer program to calculate the response of a plasma to a pulsed electron beam. The single-page program (written in BASIC) uses the two-step Lax-Wendroff method to solve Eqs. (12.67), (12.68) and (12.69). The program applies symmetry conditions at $X = 0$ and absorbing boundary conditions at $X = 1$. The division of the advancing routine into two steps is easy to see. Some other features of the program include:

Lines 132-192: Absorbing wall.

Lines 193-194: Boundary conditions at wall.

Line 200: Boundary condition on symmetry axis.

Lines 1000-1040 and 1250-1280: Numerical integration to find electric field.

Lines 1750: Subroutine to give beam density as a function of time, $g(\tau)$.

For numerical stability, the spatial and temporal steps must satisfy the constraint:

TABLE 12.1. Solution of One-dimensional Plasma Neutralization
(*Diagnostic, input/output and initialization routines omitted*)

```
10 REM ---PROGRAM SCNEUT---

30 REM ---DEMONSTRATION OF SPACE CHARGE NEUTRALIZATION
40 REM ---SHEET ELECTRON BEAM INJECTED INTO A PLASMA

70 REM ---MAIN TIME LOOP

80 FOR T=DTAU TO TMAX STEP DTAU

82 GOSUB 1750:REM --ION AND BEAM DENSITY AT NEXT TIME STEP
85 PRINT "----------CALCULATING AT T = ";T;"----------"

90 REM ---STEP 1. ADVANCE TO INTERMEDIATE POSITION

100 FOR K=0 TO NMESH:REM K=J+1/2
110 NI(K)=(N(K)+N(K+1))/2 - DTAU*(N(K+1)*V(K+1)
     - N(K)*V(K))/(2*DX)
115 IF NI(K)<0 THEN LET NI(K)=0
120 VI(K)=(V(K)+V(K+1))/2 - DTAU*(E(K)+E(K+1))/2
     - DTAU*(V(K+1)^2-V(K)^2)/(4*DX)
130 NEXT K
132 IF VI(NMESH)<0 THEN LET VI(NMESH)=0
140 GOSUB 1250:REM EVALUATE EI(K)

150 REM ---STEP 2. ADVANCE TO NEXT TIME POSITION
160 FOR J=1 TO NMESH
170 N(J)=N(J) - DTAU*(NI(J)*VI(J)-NI(J-1)*VI(J-1))/DX
175 IF N(J)<0 THEN LET N(J)=0
180 V(J)=V(J) - DTAU*(EI(J)+EI(J-1))/2
    - DTAU*(VI(J)^2-VI(J-1)^2)/(2*DX)
190 NEXT J

192 IF V(NMESH)<0 THEN LET V(NMESH)=0:
     V(NMESH+1)=V(NMESH):N(NMESH)=0
193 V(NMESH+1)=V(NMESH)
194 N(NMESH+1)=N(NMESH):E(NMESH+1)=E(NMESH)
200 N(0)=N(1):V(0)=0:E(0)=0

205 GOSUB 1000

206 ND=ND+1
207 IF ND=NDIAG THEN GOSUB 1500:ND=0: REM --DIAGNOSTICS
220 NEXT T
230 END

1000 REM ---SUBROUTINE TO CALCULATE E(J)
1010 E(0)=0
1020 FOR J=1 TO NMESH:
     E(J)=E(J-1)+DX*((NION(J)+NION(J-1)-N(J)-N(J-1))/2):NEXT J
1030 E(NMESH+1)=E(NMESH)
1040 RETURN

1250 REM ---SUBROUTINE TO CALCULATE EI(K) WHERE K=J+1/2
1260 EI(0)=DX*(NION(0)-NI(0))/2
```

```
1270 FOR K=1 TO NMESH:
     EI(K)=EI(K-1)+DX*(NION(K)-(N(K)+N(K-1))/2):NEXT K
1280 RETURN

1750 REM --SUBROUTINE ION AND BEAM DENSITY
1760 REM ---LINEAR RISE TO NB IN TIME TINJ
1765 IF T < TINJ THEN GOTO 1780
1770 FOR J=0 TO INT(XB*NMESH):NION(J)=1-NB*T/TINJ:NEXT J
1780 RETURN
```

$$\Delta\tau < \Delta X/V(j,n). \tag{12.84}$$

When the calculation goes unstable, small variations in quantities grow in a non-physical manner. The origin of the numerical instability is easy to understand by inspecting Eq. (12.84). If $V(j,n)\Delta\tau$ is greater than ΔX, electrons travel more than one spatial mesh length in a time-step. The interval $\Delta\tau$ is not short enough to fix the mesh location of electrons unambiguously at each time-step, leading to non-physical transport mechanisms.

Figures (12.9) and (12.10) show histories of normalized density, directed velocity and electric field for a beam density uniform in the range $0 < X < (x_o/x_w)$ with time variation:

$$N_b(\tau) = N_{bo}(\tau/\tau_b), \ (0 \le \tau < \tau_b), \tag{12.85}$$

$$= N_{bo}, \ (\tau \ge \tau_b).$$

The dimensionless form of the equations helps to pick appropriate run parameters. For example, the condition of a fast-rising beam density is:

$$\tau_b = \omega_{pe}\Delta t_b \ll 1. \tag{12.86}$$

Figure 12.9 shows results for an instantaneous rise of beam density, $\tau_b = 0$. The beam has $N_{bo} = 0.25$ and $(x_o/x_w) = 0.25$. The spatial resolution is $NMesh = 25$ ($\Delta X = 0.04$). The maximum space-charge imbalance in the system at any time is less than 0.25. Therefore the directed velocity lies in the range $V(j,n) < 0.5$. We take a time-step of $\Delta\tau = 0.05$ to guarantee stability. Despite its simplicity, the model gives interesting results. Figure 12.9 confirms the contention of Section 12.2 that a beam with a fast rise time ($\tau_b \le 1/\omega_{pe}$) creates a large space-charge imbalance. The solution shows high directed plasma electron velocity and large electric fields. Note the inward and outward propagation of a plasma disturbance. As expected, the bounce period in dimensionless time units equals 2π.

Figure 12.10 shows a calculation with a longer beam rise time, $\tau_b = 12$. The directed velocity and electric field are much smaller. By the end of the run ($\tau = 16$), the plasma density has adjusted to the presence of the beam – at the center it is lower by a factor of 0.75. The large electron density spikes result from the interference of plasma waves – the divergences would disappear if we added effects of electron temperature to the moment equation model.

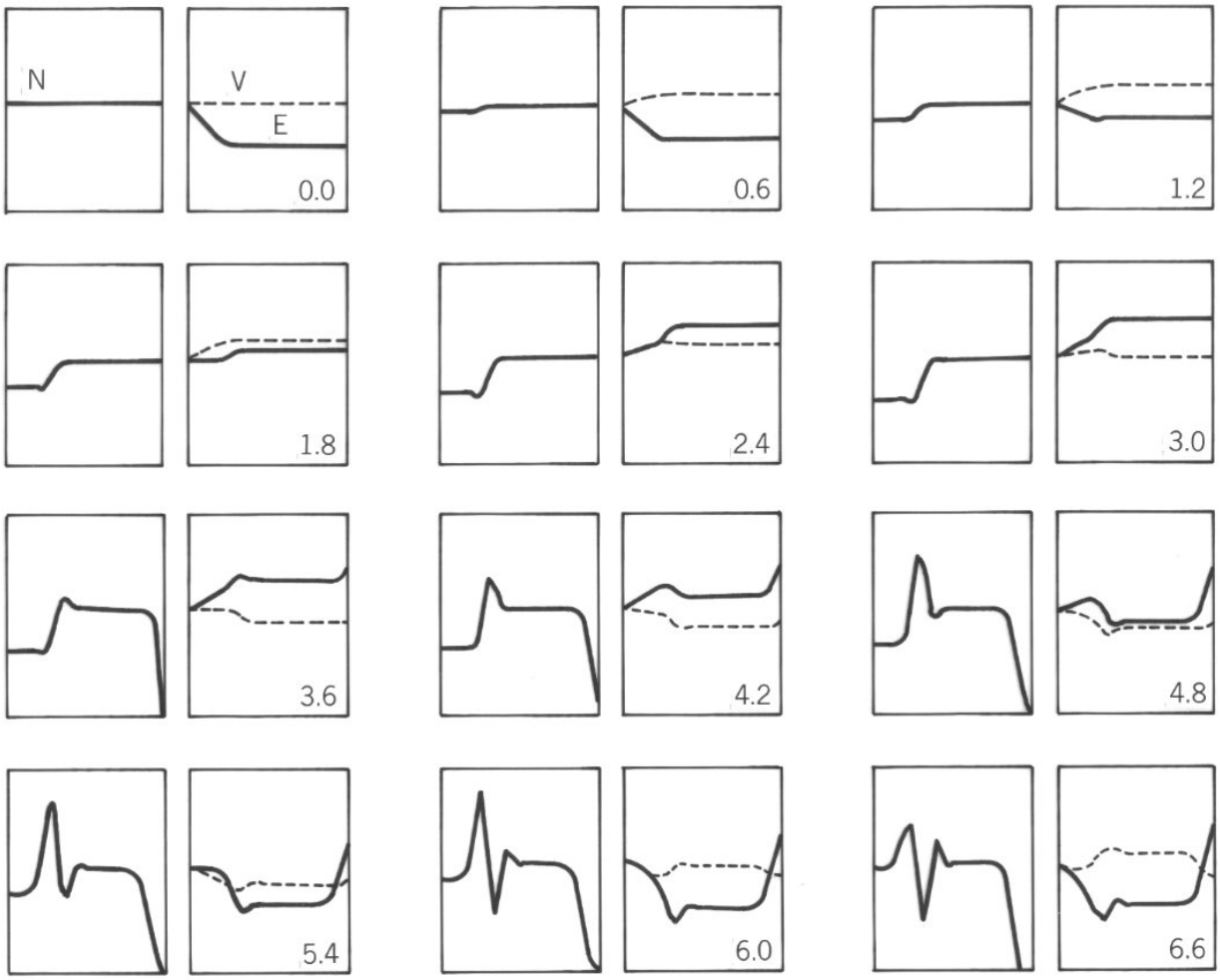

Figure 12.9. History of the normalized plasma electron density (N), directed velocity (V) and electric field ($\boldsymbol{E}$) as a function of τ following instantaneous injection of a high energy sheet electron beam. The figure gives plots of the spatial variation of N, V and $\boldsymbol{E}$ at several values of τ. N_{bo}= 0.25, X_b = 0.25, τ_b = 0, ΔX = 0.04, $\Delta\tau$ = 0.05.

12.5. Magnetic skin depth

A rapidly-pulsed electron beam induces current in a conductive plasma. The plasma current opposes the beam current and may interfere with self-pinched propagation of the beam. A pulsed beam entering a plasma creates a changing magnetic field. The resulting inductive electric field accelerates plasma electrons in the direction opposite to that of the beam electrons. If the plasma current density has about the same spatial distribution as the beam current density, the plasma cancels the beam-generated magnetic field – the beam is *current neutralized*.

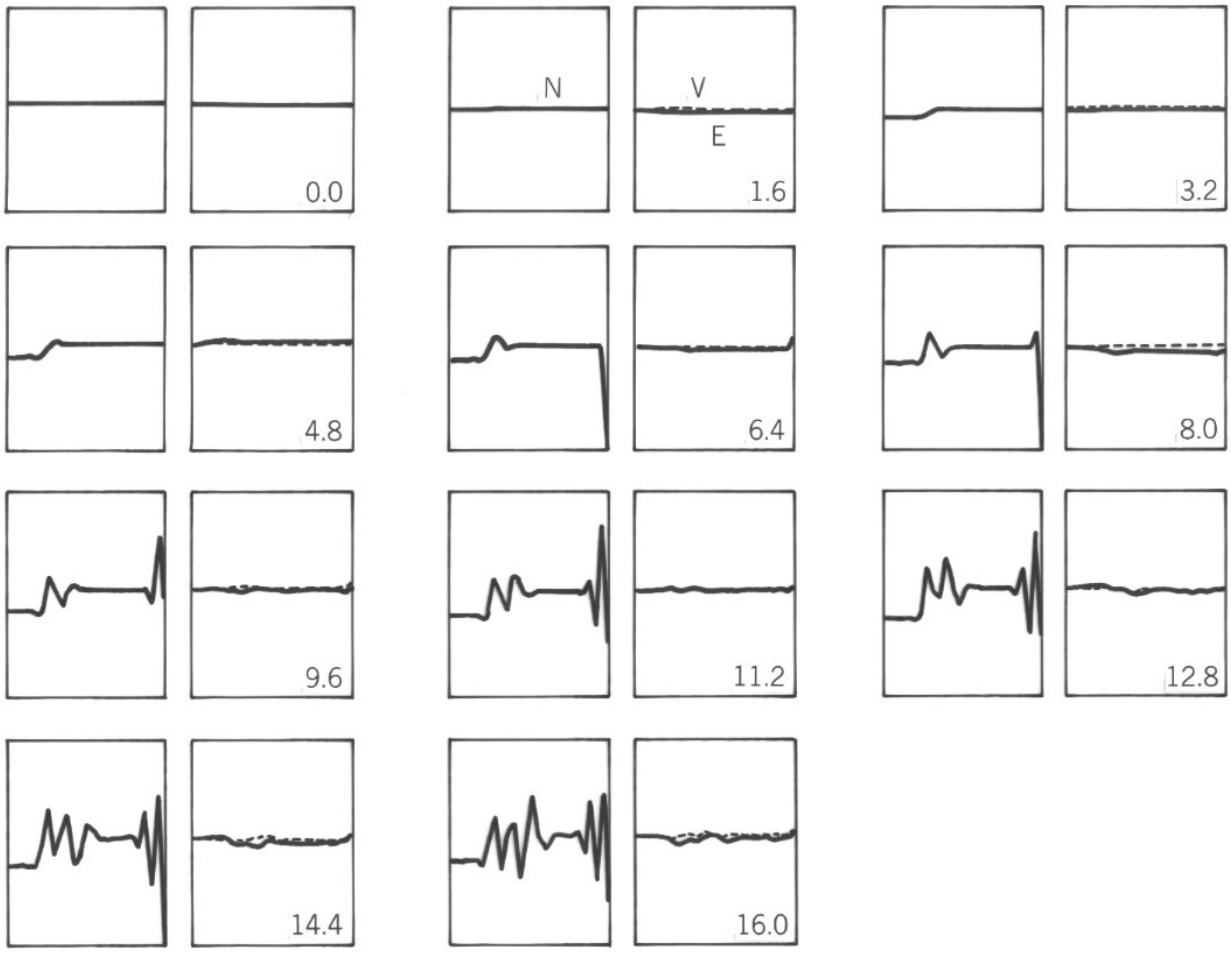

Figure 12.10. History of the normalized plasma electron density (N), directed velocity (V) and electric field ($\boldsymbol{E}$) as a function of τ following slow injection of a high energy sheet electron beam. $N_{bo}= 0.25$, $X_b = 0.25$, $\tau_b = 12$, $\Delta X = 0.04$, $\Delta\tau = 0.05$.

To understand the response of a plasma to a changing magnetic field we shall study the simplified geometry of Figure (12.11). A coil produces a pulsed magnetic field outside the sharp boundaries of a uniform density plasma with infinite extent in the y and z directions. The plasma has width L and equal electron and ion densities, $n_e = n_i = n_o$. Following Figure 12.11, the magnetic fields are symmetric about the line $x = L/2$. Outside the plasma the magnetic field is a specified function of time $B_o(t)$ given by the variation of coil current. We want to find the distribution of magnetic field inside the plasma as a function of position and time, $B_z(x,t)$.

A perfectly-conducting plasma excludes the applied magnetic field for all time. With plasma collisional resistivity the field ultimately penetrates the plasma (Sect.ion12.6). Even with no collisions magnetic fields can penetrate a distance into the plasma because of the electron inertia. The penetration distance is called the *magnetic skin depth*.

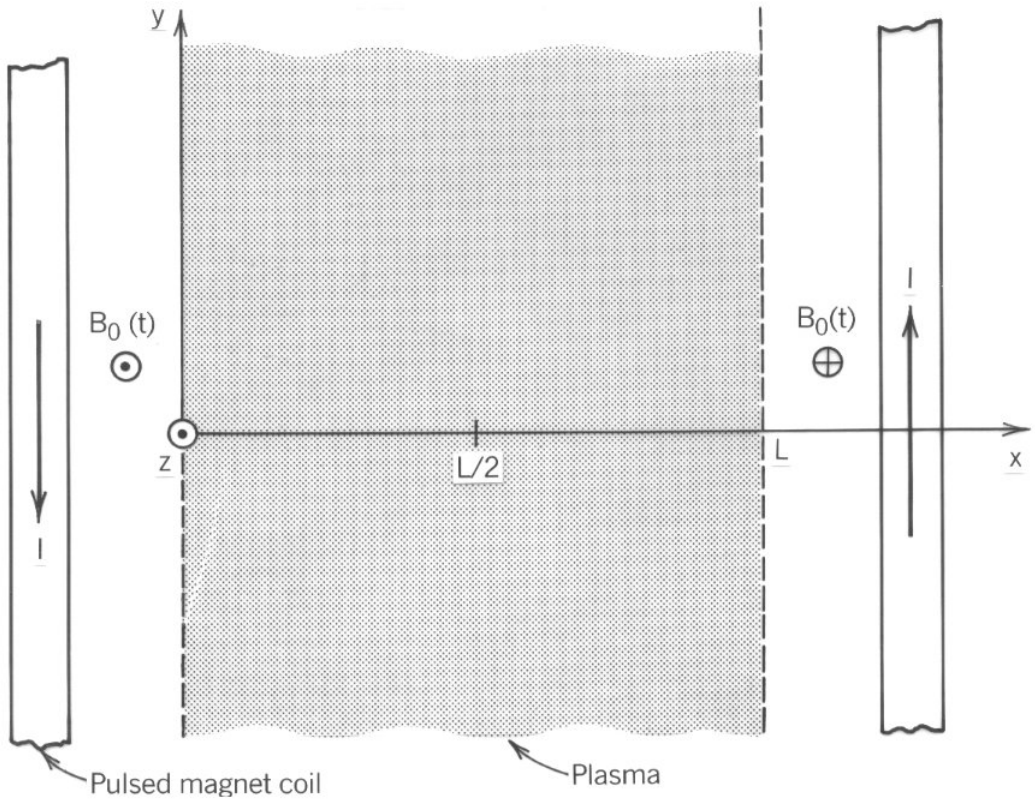

Figure 12.11. Schematic geometry to calculate the magnetic skin depth of a homogeneous plasma.

In calculating the response of a zero-resistivity plasma to a pulsed magnetic field, we initially neglect the motion of massive plasma ions. We shall concentrate on the left-hand boundary of Figure 12.11. The coil current moves in the -y direction, generating an applied magnetic field in the +z direction. The inductive electric field accelerates plasma electrons in the -y direction – the plasma current flows in the +y direction. The plasma current opposes the applied current, excluding magnetic field from the plasma volume. For a given spatial variation of plasma electron current density at time t, $j_{ey}(x,t)$, Eq. (1.31) determines the spatial variation of magnetic field:

$$\frac{\partial B_z(x,t)}{\partial x} = -\mu_o\, j_{ey}(x,t)\ . \tag{12.87}$$

Electric fields in the plasma result from a changing magnetic flux. With the symmetry of Figure 12.11, the total magnetic flux enclosed within position x at time t for a unit length in the y direction is the integral over x of $B_z(x,t)$ from $x = 0$ to $x = L/2$. In the limit of strong field

exclusion at the center of the plasma the integral can extend to +∞ with little loss in accuracy. Faraday's law is:

$$E_y(x,t) = -\int_x^\infty dx' \frac{\partial B_z(x',t)}{\partial t} . \tag{12.88}$$

To simplify the calculation, we shall temporarily neglect the effect of the magnetic field on the electron orbits – electrons move only in the -*y* direction. The acceleration is:

$$\frac{\partial v_{ey}(x,t)}{\partial t} = -\frac{eE_y(x,t)}{m_e} = -\int_x^\infty dx' \frac{e}{m_e} \frac{\partial B_z(x',t)}{\partial t} . \tag{12.89}$$

We can integrate both sides of Eq. (12.89) over time *t*'. The integration extends from *t*' = 0 to the time of interest, *t*' = t. If $B_o(0) = 0$, then $v_{ey}(x,0) = 0$ and $B_z(x,0) = 0$. With these conditions, the integration gives:

$$v_{ey}(x,t) = -\frac{j_{ey}(x,t)}{en_o} = -\frac{e}{m_e} \int_x^\infty dx' B_z(x',t) . \tag{12.90}$$

The derivative of Eq. (12.90) with respect to *x* is:

$$\frac{\partial j_{ey}(x,t)}{\partial x} = \frac{-e^2 n_o B_z(x,t)}{m_e} . \tag{12.91}$$

Combining Eqs. (12.87) and (12.91) gives an equation for the spatial variation of B_z at time *t*:

$$\frac{\partial^2 B_z(x,t)}{\partial x^2} = \frac{\mu_o e^2 n_o B_z(x,t)}{m_e} = \frac{e^2 c^2 n_o B(x,t)}{\epsilon_o m_e} . \tag{12.92}$$

With the boundary condition $B_z(0,t) = B_o(t)$, the solution of Eq. (12.92) is:

$$B_z(x) = B_o \exp(-x/\lambda_m). \tag{12.93}$$

The quantity λ_m is the magnetic skin depth:

$$\lambda_m = c/(e^2 n_o/\epsilon_o m_e)^{1/2} = c/\omega_{pe}. \tag{12.94}$$

The final form of Eq. (12.94) incorporates the electron plasma frequency [Eq. (12.23)]. Because

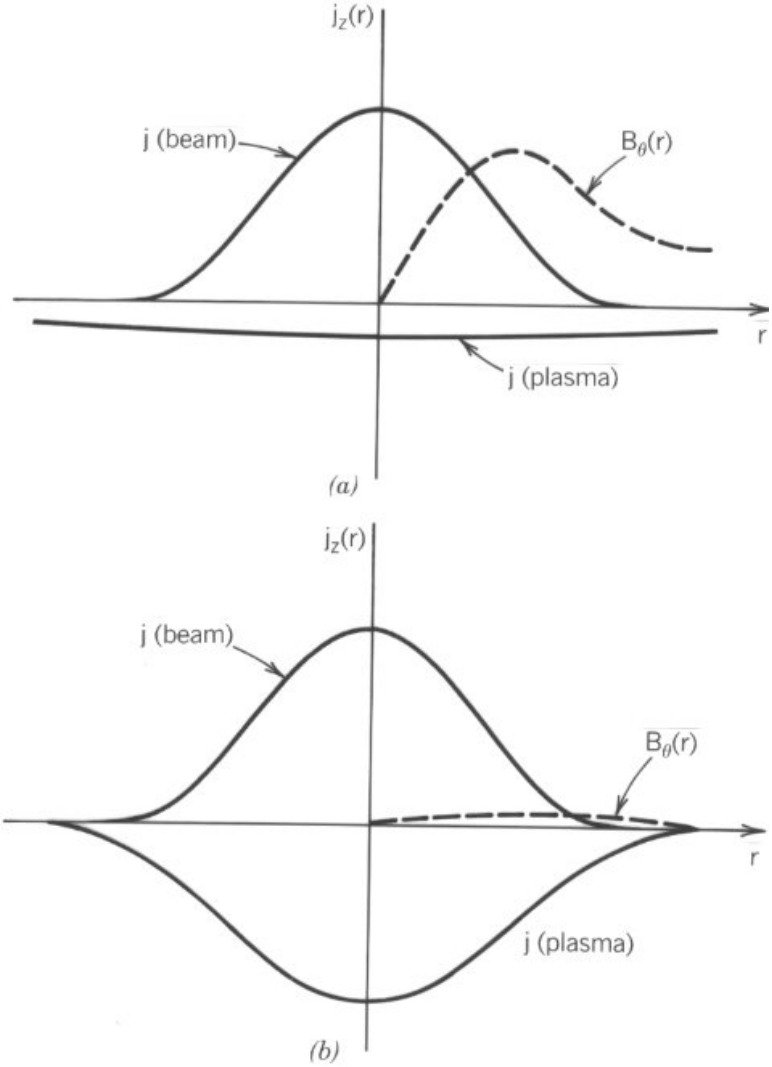

Figure 12.12. Spatial profiles of beam current-density, plasma current-density, and toroidal magnetic field following injection of a cylindrical electron beam into a plasma with zero resistivity. *a*) $r_b \ll \lambda_m$. *b*) $r_b \ll \lambda_m$.

of electron inertia a magnetic field penetrates into zero-resistivity plasma a distance comparable to λ_m. As an example a plasma with density 10^{19} m^{-3} has an electron plasma frequency of $\omega_{pe} = 1.8 \times 10^{11}$ m^{-3}. Substitution in Eq. (12.94) gives a collisionless skin depth of $\lambda_m = 1.6$ mm.

Figure 12.12 shows the significance of λ_m for the current neutralization of a pulsed electron beams. Usually the plasma frequency is high enough to guarantee complete space-charge neutralization during the rise of beam current. If the beam propagates in plasma with no nearby conducting boundaries, the net plasma current has magnitude equal to that of the beam current. If

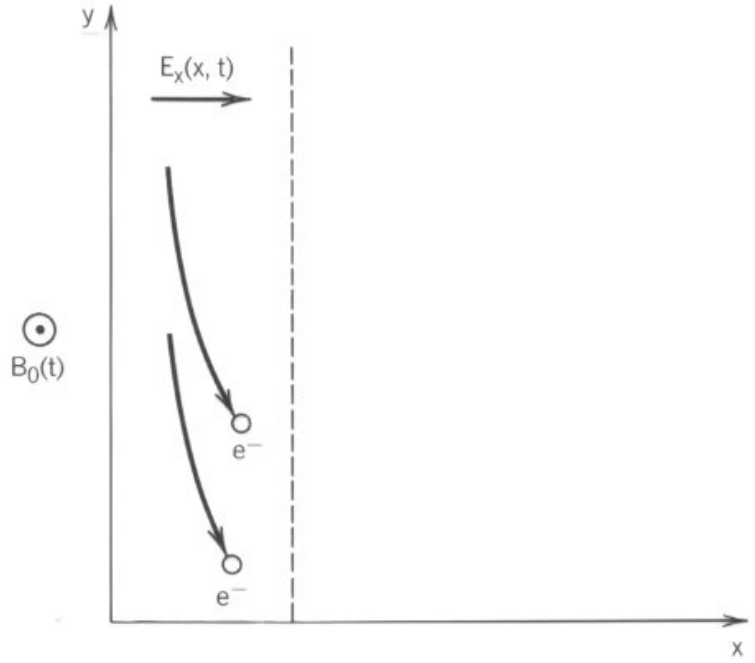

Figure 12.13. Mechanism for the magnetic acceleration of a plasma. The plasma has a boundary at x = 0 and extends over the region $x > 0$. A pulsed magnetic field fills the region $x < 0$. Dashed line shows region of induced electron current extending to $x \sim \lambda_m$.

the beam radius is smaller than λ_m the plasma return current occupies a larger cross-section area than the beam (Figure 12.12*a*). As a result, the magnetic field inside the beam almost equals the value of the beam-generated field without the plasma – the beam can propagate in a self-pinched equilibrium. In the opposite limit of large beam radius the spatial distributions of beam and plasma current density are almost the same. Figure 12.12*b* shows that the net magnetic field inside the beam almost equals zero.

We can apply the result of Eq. (12.94) to calculate the magnetic acceleration of a plasma. This process is often applied in pulsed plasma guns for intense ion beam extraction. Here we must include effects of magnetic bending of electron orbits and acceleration of ions by the resulting charge separation. Figure 12.13 shows the behavior of particles at the boundary between a plasma and a rising magnetic field. The field generates an electron current localized to a surface layer of width λ_m. The magnetic field in the layer also exerts an x-directed force on the electrons. The electrons shift away from the ions in the layer creating an electron field $E_x(x,t)$. The flow of electrons approaches an instantaneous force equilibrium if the electric field has the value:

$$E_x(x,t) \cong v_{ey}(x,t)\, B_z(x,t). \tag{12.95}$$

The electric field accelerates ions, resulting in a long-term motion of the plasma boundary. We

can estimate the velocity of the plasma by applying the condition of global force balance over the current sheath. The force per volume in the sheath is $j_{ey}B_z$ (newtons/m^3). The force per area on the plasma equals the integral of the volume force over the sheath width:

$$F_a(t) = \int_0^\infty dx\; j_{ey}(x,t)\; B_z(x,t)\;. \tag{12.96}$$

Equations (12.91) and (12.93) imply that the electron current density has the following variation with depth in the plasma:

$$j_{ey}(x,t) \cong (e^2 n_o \lambda_m / m_e)\, B_o(t) \exp(-x/\lambda_m). \tag{12.97}$$

Substituting Eqs. (12.93) and (12.97) in Eq. (12.97) gives an expression for total force per area on the plasma:

$$F_a = B_o^2(t)/2\mu_o. \tag{12.98}$$

Equation (12.98) is the familiar expression for the magnetic pressure exerted by the field B_o(t) on a highly-conducting body.

The inertia of ions governs the velocity of the plasma front. Suppose that the boundary moves in the $+x$ direction at velocity v_d. In the single-particle limit we expect that ions gain a velocity $2v_d$ in an elastic reflection from the moving front. On the other hand experiments show that accelerated ions streaming through a plasma are subject to strong momentum transfer instabilities. As a result ions are swept up and carried with the moving front at about velocity v_d. If the ion density is n_o the change of plasma momentum per area per time equals the momentum gain of a single ion multiplied by the number of ions swept up by the moving front per unit time in a unit cross-sectional area:

$$dp_a/dt = (m_i v_d)\,(n_o v_d). \tag{12.99}$$

Equating the rate of change of plasma momentum to the magnetic force gives the following expression for the plasma front velocity:

$$v_d = \left[\frac{B_o^2}{2\mu_o n_o m}\right]^{1/2}. \tag{12.100}$$

The quantity v_d of Eq. (12.100) is called the *Alfven velocity*. For a plasma of density 10^{19} m^{-3} and an applied field of 0.10 tesla, the Alfven velocity equals 1.41×10^5 m/s for C^+ ions. The velocity corresponds to a directed ion kinetic energy of 2.5 keV. The available pulsed current density of C^+ ions is $j_i \cong en_o v_d = 23 \times 10^4$ A/m^2. This value is much higher than those from steady-state ion sources (Section 7.6).

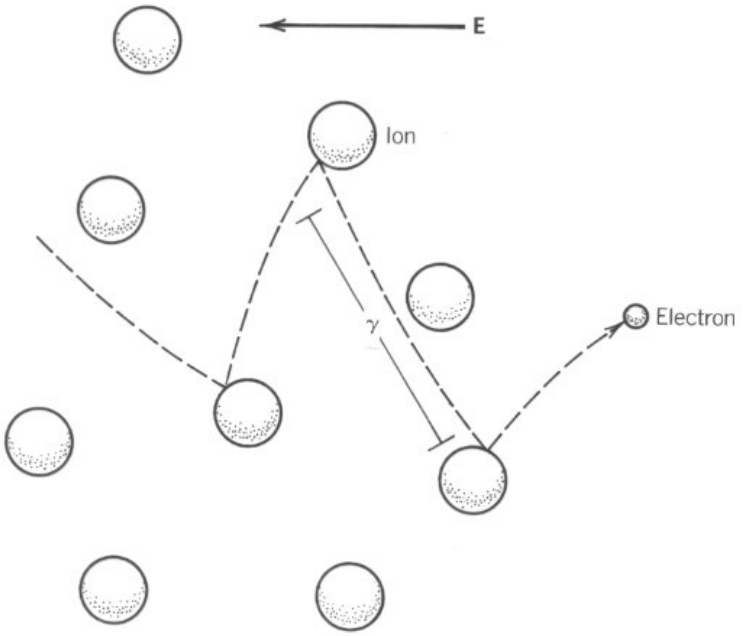

Figure 12.14. Definition of mean-free-path for collisions of free electrons with background atoms.

12.6. Return current in a resistive plasma

Section 12.5 showed that the magnetic fields of a rapidly-pulsed electron beam entering a plasma are almost completed neutralized in the limit $r_o \gg \lambda_m$. Inductive axial electric fields create a plasma return current – a small reduction of the beam kinetic energy supplies the energy of the plasma current. If the beam current stays roughly constant for $t > 0$, the spatial distribution of return current may change with non-zero plasma resistivity. In this section we shall study the nature of plasma resistivity. First we shall derive expressions for resistivity and then develop equations describing the time-variation of plasma current density. The section concludes with a discussion of implications of the diffusion equation, including wake effects.

The cold plasmas that are often used for high-current electron beam propagation are poor conductors compared with metals. Plasma resistivity can lead to significant perturbations of the return current even for short pulsed electron beams. Resistance results from collisions that interrupt the directed plasma electron motion. Collisions with neutrals are important in weakly-ionized plasmas – at high current density electrons can exchange momentum with plasma ions through collective instabilities. In this section we shall concentrate on the resistivity of a fully-ionized plasma with no applied magnetic field. The current density is moderate – momentum transfer to ions occurs through *Coulomb collisions*. These collisions are electric field electric field deflections that occur when an electron passes close to an ion. The model holds when the electron drift velocity v_d that produces the plasma current is smaller than the randomly-directed electron thermal velocity v_{th}. In this limit the current density is proportional to the applied

electric field and the electron flow is stable against the two-stream instability.

Collisions between electrons cannot change the average momentum of a drifting electron distribution. Momentum transfer takes place between the electrons and stationary ions. We define the mean-free-path for momentum transfer λ as the average directed distance an electron travels before a collision with an ion. In the simplified representation of Figure 12.14 an applied electric field accelerates electrons. They lose their directed momentum through a collision with an ion after moving an average distance λ. When $v_{th} \gg v_d$ the thermal velocity determines the time between collisions:

$$\Delta t \cong \lambda / v_{th}. \tag{12.101}$$

The collision frequency for momentum transfer to ions υ_{ei} is the inverse of Δt,

$$\nu_{ei} \cong 1/\Delta t = v_{th}/\lambda. \tag{12.102}$$

If electrons freely accelerate between collisions, the average directed velocity superimposed on the random thermal velocity is:

$$\boldsymbol{v_d} = \nu_{ei} \int_0^{1/\nu_{ei}} dt' \, \frac{-eE\ t'}{m_e} = -\frac{eE}{2m_e \nu_{ei}} \ . \tag{12.103}$$

For a uniform electron density n_o the current density associated with the drift velocity is $\mathbf{j}_e = -en_o\mathbf{v}_d$, or

$$\mathbf{j}_e = (e^2 n_o / 2m_e \nu_{ei})\ \mathbf{E}. \tag{12.104}$$

Equation (12.104) shows that plasma electron flow satisfies Ohm's law:

$$\mathbf{E} = \rho\ \mathbf{j}_e. \tag{12.105}$$

if we take the volume resistivity as:

$$\rho = 2m_e \nu_{ei} / e^2 n_o\ (\Omega\text{-m}). \tag{12.106}$$

An analysis of the deflection of electrons traveling past ions leads to an estimate of the collision frequency in a fully ionized plasma [See, for instance, D.J.Rose and M. Clark, **Plasmas and Controlled Fusion** (MIT Press, Cambridge, 1961), p. 167]. For physically-correct results it is necessary to include plasma shielding effects for the ion charge at distances greater than the Debye length λ_d. The following equation applies to a plasma with singly charged ions and a Maxwell distribution of electron velocities with temperature T_e:

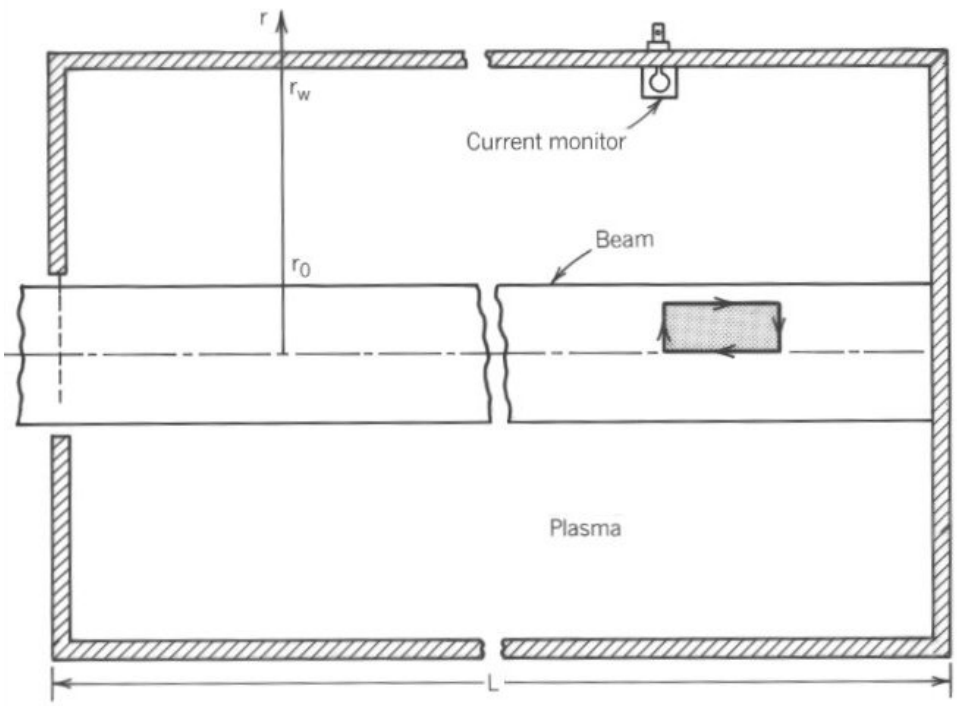

Figure 12.15. Geometry for the calculation of the radial distribution of return current for a cylindrical pulsed electron beam in a plasma-filled chamber.

$$\nu_{ei} = \frac{e^4 \, n_o \, \ln(\Lambda)}{32 \sqrt{2\pi m_e} \, \epsilon_o^2 \, (kT_e)^{3/2}} \, . \tag{12.107}$$

The quantity Λ is the *plasma parameter*:

$$\Lambda = 12\pi \frac{(\epsilon_o \, kT_e / e^2)^{3/2}}{n_o^{1/2}} = 9\left[\frac{4\pi n_o \, \lambda_d^3}{3}\right] . \tag{12.108}$$

The final form on the right-hand side of Eq. (12.108) shows that Λ is proportional to the number of particles within a spherical volume of radius λ_d, the *Debye sphere*. A group of charged particles acts like a plasma when there are many particles in a Debye sphere. To illustrate the application of Eqs. (12.106) and (12.107) suppose we have an ion source plasma with a density of 10^{19} m^{-3} and an electron temperature of kT_e = 10 eV. For the Debye length of 7.44 μm, there are over 5000 particles in a Debye sphere. The plasma parameter is Λ = 10.8, giving a collision frequency of 5.8×10^6 s^{-1}. Finally the volume resistivity is $\rho = 4.2 \times 10^{-5}$ Ω-m. In comparison, the volume resistivity of pure copper is $\rho = 1.7 \times 10^{-8}$ Ω-m.

Knowing ρ we can find the variation of plasma return current near a pulsed electron beam.

Figure 12.15 illustrates the geometry of the calculation. A cylindrical electron beam of radius r_o enters a plasma with $\lambda_m \ll r_o$. We neglect the effects of plasma electron inertia – the plasma acts as an ideal resistor with no phase shift between **j** and **E**. Also the plasma completely cancels beam-generated electric fields. Our model treats only variations in in the radial direction – the following assumptions allow the neglect of axial variations:

1. The beam traverses a plasma-filled chamber with conducting walls. The chamber has length L and a large wall radius $r_w \gg r_o$.

2. The time scale for changes in the plasma current density is much longer than the beam transit time through the chamber $L/\beta c$.

3. The beam is paraxial and axially uniform.

If the electron beam has a fast rise-time the plasma return current density $j_e(r)$ initially has the same spatial variation as that of the beam $j_b(r)$. Therefore there is no beam-generated magnetic field at $t = 0$.

When ρ is non-zero an axial electric field must be present to maintain the return current:

$$E_z(r) = \rho\, j_e(r). \tag{12.109}$$

The only possible source of the electric field is a changing magnetic flux because the ends of the chamber are electrically connected. The magnetic field points in the azimuthal direction. To calculate the electric field we apply Faraday's law to the loop shown in Figure 12.15. Noting that $E_z(0) = 0$, the electric and magnetic fields are related by:

$$\int_0^r dr' \left(\frac{\partial B_\theta(r)}{\partial t} \right) \Delta z = E_z(r)\ \Delta z. \tag{12.110}$$

The magnetic field results from the sum of beam and plasma currents:

$$B_\theta(r) = \frac{\mu_o}{2\pi r} \int_0^r 2\pi r' dr' \left[j_b(r') + j_e(r') \right] . \tag{12.111}$$

The radial derivative of Eq. (12.110) is:

$$\partial B_\theta(r)/\partial t = \partial E_z(\mathrm{r})/\partial r = \rho(r)\, \partial j_e(\mathrm{r})/\partial \mathrm{r}. \tag{12.112}$$

Taking partial derivatives of Eq. (12.111) with respect to radius and time gives the relationship:

$$\frac{\partial j_b}{\partial t} + \frac{\partial j_e}{\partial t} = \frac{1}{\mu_o}\frac{1}{r}\frac{\partial}{\partial r}\left(r\frac{\partial B_\theta}{\partial t}\right) . \tag{12.113}$$

Combining Eqs. (12.112) and (12.113) leads to an equation that describes the spatial and temporal variation of plasma current density:

$$\frac{\partial j_e(r,t)}{\partial t} = \frac{1}{\mu_o}\frac{1}{r}\frac{\partial}{\partial r}\left(r\rho(r,t)\frac{\partial j_e(r,t)}{\partial r}\right) - \frac{\partial j_b(r,t)}{\partial t} . \tag{12.114}$$

Equation (12.114) has the form of the familiar diffusion equation. The diffusion constant is $D(r,t) = \rho(r,t)/\mu_o$. The given beam current density acts as a source term for the plasma return current.

We can solve Eq. (12.114) when the resistivity has a constant value in space and time, $\rho(r,t) = \rho_o$, and the beam current density follows a step function temporal variation. The beam current density rises instantaneously at $t = 0$. Because $j_b(t)$ is constant for $t > 0$ we can remove the source term from Eq. (12.114) – the beam sets the initial condition $j_e(\underline{r},0) = -j_b(r,0)$. The equation has the form:

$$\frac{\partial j_e}{\partial t} = \left[\frac{\rho_o}{\mu_o}\right]\nabla^2 j_e . \tag{12.115}$$

The symbol ∇^2 represents the Laplace operator appropriate for the geometry of the problem.

The diffusion equation is one of the most familiar relationships in collective physics. It describes a wide array of phenomena, such as the flow of heat in solids and the diffusion of neutrons. Many analytic solutions to Eq. (12.115) have been tabulated [see, for example, H.S. Carslaw and J.C. Jaeger, **Conduction of Heat in Solids, Second Edition** (Clarendon Press, Oxford, 1959). For example suppose we have a narrow cylindrical beam that enters a plasma with uniform resistivity ρ_o. The beam current rises instantaneously to I_o at time $t = 0$. If we can approximate the narrow beam as an on-axis current filament, then the plasma return current outside the beam has the spatial and temporal variations:

$$j_e(r,t) = \left[\frac{I_o\ \rho_o}{4\pi\mu_o\ t}\right]\exp\left[\frac{-r^2\rho_o}{4\mu_o\ t}\right] . \tag{12.116}$$

We can verify the validity of Eq. (12.116) by direct substitution into Eq. (12.115). The integral of j_e over all radii always equals $-I_o$. If we define the average radius of the plasma current as the point where j_e falls to 1/e of its peak value, then Eq. (12.116) implies that:

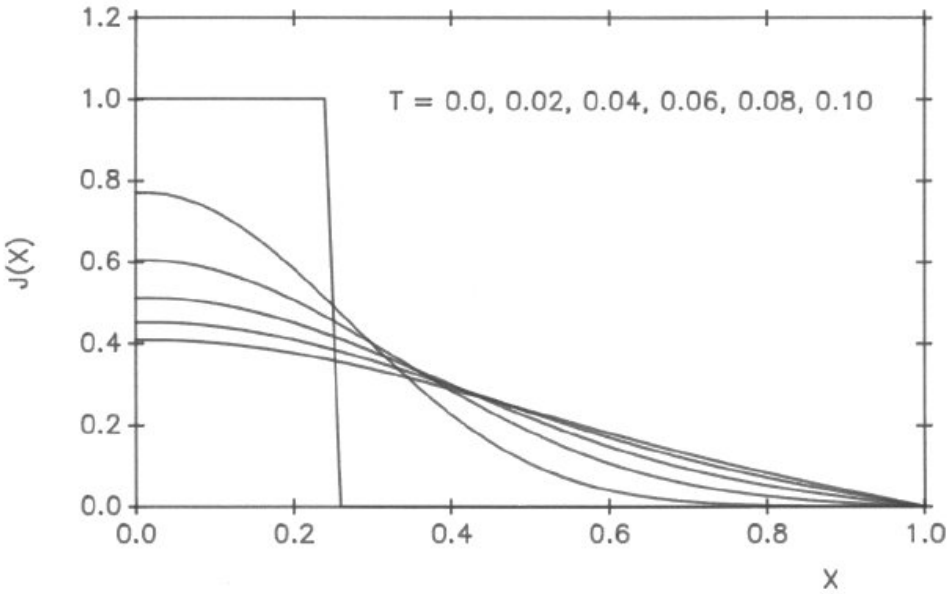

Figure 12.16. Numerical solutions to the equation $\partial^2 J/\partial X^2 = -\partial J/\partial T$ for an initial step function variation of J. Symmetry axis at $X = 0.0$, absorbing wall at $X = 1.0$. Spatial mesh: $dX = 0.02$. Solution time step: $dT = 0.0001$.

$$\langle r \rangle = \sqrt{4\mu_o t/\rho_o} \ . \tag{12.117}$$

Expansion of the plasma current is proportional to the square-root of time.

We can also solve Eq. (12.115) numerically. This approach is often necessary if the plasma conductivity varies with position and time. Defining the current density on a radial mesh with $r_i = i\,\Delta r$, the finite difference form of Eq. (12.115) is:

$$\frac{\partial j_i}{\partial t} \cong \left[\frac{1}{\mu_o}\right]\left[\frac{(j_{i+1}-j_i)\rho[(i+0.5)\Delta r] \ - \ (j_i-j_{i-1})\rho[(i-0.5)\Delta r]}{i\ \Delta r^2}\right] \tag{12.118}$$

We can apply time-centered methods for partial differential equations (Section 12.4) to solve Eq. (12.118). Usually, the time step must be in the range $\Delta t < \Delta r^2/(\rho/\mu_o)$ for numerical stability.

Figure 12.16 shows results of a numerical solution of the diffusion equation. In the calculation, a sheet beam with a rapid rise time has uniform current density j_b from the axis to $x = x_o = x_w/4$. The beam propagates through a uniform plasma with constant resistivity between plates at $x = \pm x_w$. Initially, the plasma current density has the same spatial profile as the beam. Later, the plasma current spreads over a larger area.

The time scale for significant spreading of the plasma current from a cylindrical beam of radius r_o is the *current decay time*:

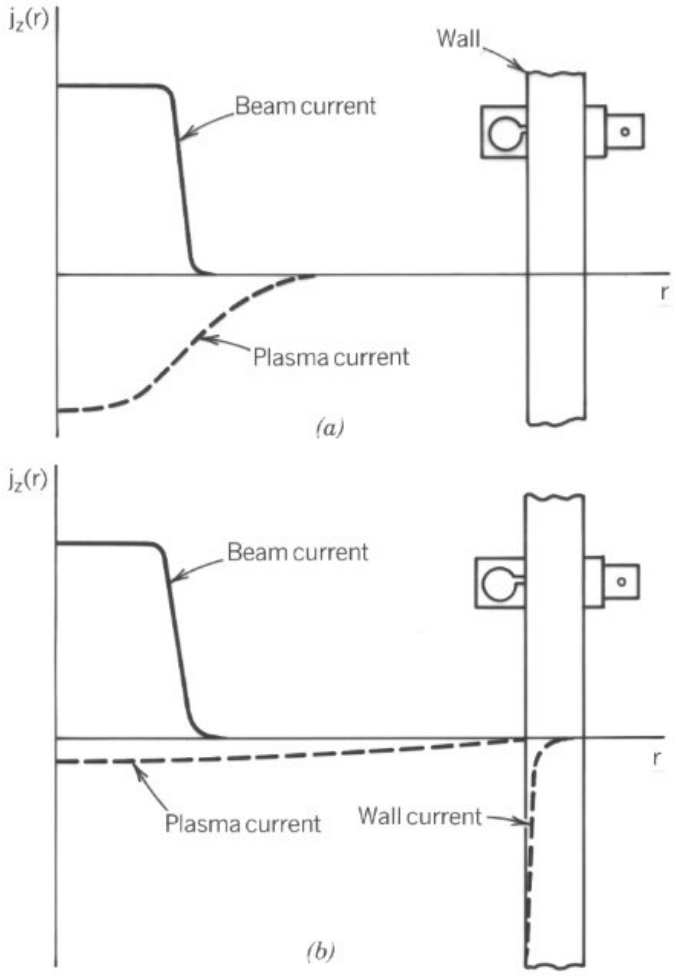

Figure 12.17. The radial distribution of return current for a pulsed cylindrical electron beam in a plasma-filled chamber. *a*) Immediately after beam injection, the plasma current has almost the same spatial distribution as that of the beam. *b*) Later in time, the plasma current density distribution is diffuse and the wall carries some of the current.

$$\tau_d \cong \mu_o r_o^2/\rho_o. \tag{12.119}$$

The diffusion of the plasma return current involves the interaction between inductive and resistive effects. At $t = 0$ the distribution of return current minimizes the inductance for the plasma current. Later the plasma current spreads to minimize the resistance. If the plasma current expands to an area significantly larger than that of the beam, the azimuthal magnetic field in the beam volume approaches the value without plasma. The quantity τ_d also represents the time scale for the decay of plasma current in the beam volume. For a resistivity of $\rho = 4.2 \times 10^{-5}$ Ω-m and a beam radius of $r_o = 0.01$ m, the current-neutralization decay time is $\tau_d = 3$ μs.

We must be careful analyzing the interactions of intense electron beams ($\gg$1 kA) with plasmas. These beams can deposit energy in the plasma, raising the electron temperature and lowering the local resistivity [Eq. (12.106)]. The region occupied by the beam may have high conductivity while the surrounding cold plasma is resistive. Intense electron beams induce strong plasma

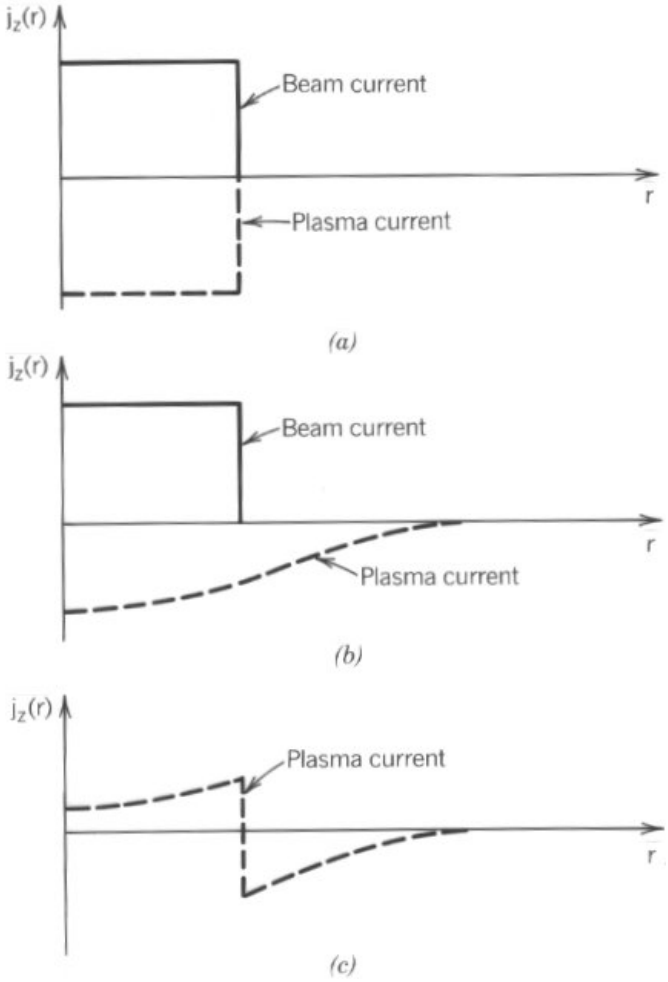

Figure 12.18. Wake fields generated by a pulsed electron beam in a chamber filled with a resistive plasma. Solid line: radial distribution of beam current density. Dashed line: radial distribution of plasma current density. *a*) Immediately following injection. *b*) Late in the beam pulse. *c*) After the beam pulse has passed.

currents. If the plasma electron drift velocity exceeds the thermal velocity the electrons may exchange momentum with the plasma ions through collective instabilities. For example suppose an electron beam with $j_b = 1000 \times 10^4$ A/m^2 enters a plasma with density 10^{19} m^{-3} and electron temperature $kT_e = 10$ eV. If plasma electrons carry a current density $-j_b$ they travel with drift velocity 6.3×10^6 m/s. In comparison, the thermal velocity is only 1.06×10^6 m/s. For these parameters we expect to observe collective interactions. The resulting *anomalous resistivity* is usually much greater than the single particle prediction of Eq. (12.106).

Most transport experiments take place inside a conducting pipes with moderate radius. In this geometry the wall can carry a portion of the return current. Figure 12.17*a* shows a simplified geometry for such an experiment. A fast-rising electron pulse enters a pipe filled with uniform-resistivity plasma. Immediately after injection, the plasma return current flows in the beam volume (Figure 12.17*b*). The net current inside the pipe equals zero – there is no changing magnetic flux to drive axial current along the pipe wall. A beam current probe (that senses B_θ) just inside the wall shows no signal. After an interval $-\tau_d$ the plasma current spreads radially

outward toward the pipe (Figure 12.17*c*). The inside wall of the conducting pipe carries a portion of the return current. The probe senses a net current in the direction of the beam current with magnitude equal to the wall current. At late time ($t \gg \tau_d$) almost all return current flows through the pipe rather than through the resistive plasma – the probe signal is close to that of the net beam current. While the net plasma return current induced by a beam decays inside a conducting induced by a beam decays inside a conducting chamber, in free space the magnitude of the plasma current always equals the beam current – only the spatial distribution changes.

When an electron beam with a finite pulse length travels through a resistive plasma it may leave behind a perturbed field distribution. The residual fields may influence electron orbits in following beam pulses. This process may lead to beam instabilities – a perturbation in a lead pulse communicates with and grows in following pulses. Electric or magnetic fields that preserve a memory of a beam pulse are called *wake fields*. Figure 12.18 illustrates the mechanism for wake field formation in a resistive plasma. The current of an electron beam with uniform current density follows a square pulse in time (Figure 12.18*a*). The pulse length Δt_b is comparable to the current decay time t_d. At time $t = 0^+$ the beam and plasma current densities have the same spatial profile – there is no magnetic field. At the end of the pulse the plasma current has expanded to a larger radius, and there is a net magnetic field within the beam (Figure 12.18*b*). When the beam current ends at $t = \Delta t_b$ the net plasma current must drop to zero. The falling beam current induces a plasma current density equal in magnitude and direction to that of the beam j_b. Fig.\ure 12.18*c* illustrates the net current density and magnetic field remaining in the plasma just after the beam passes. The opposing plasma currents ultimately diffuse together, annihilating the magnetic field. If a second beam pulse enters before field cancellation, the remaining field may deflect the electrons. The wake field results from the plasma resistivity – in a perfectly-conducting plasma the currents induced by the rise and fall of the beam current cancel exactly, leaving no sign that the that beam has passed.

12.7. Limiting current for neutralized electron beams

The main reason to propagate electron beams through a plasma is to cancel beam-generated electric fields and to allow the transport of very high currents. Section 12.6 showed that sometimes the plasma also reduces the beam-generated magnetic field. If the magnetic field is not completely canceled the beam electrons oscillate in the radial direction. At a certain value of net current the magnetic field is high enough to reverse the orbits of some beam electrons. This process sets an upper limit on the net current. The limiting value is the *Alfven current*, I_A. We have already applied the Alfven current as a scaling factor for relativistic beams (Section 10.5).

To calculate the current limit consider a cylindrical relativistic electron beam in a plasma. The beam pulselength is comparable to or greater than τ_d. Although the plasma cancels the electric field there is a magnetic field inside the beam volume. We shall not pursue a fully self-consistent model. Instead we postulate a radial variation of beam current density and investigate the properties of single particle orbits in the resulting magnetic field. The quantity I is the net current contained within the beam radius r_o. The function $F(r/r_o)$ specifies the radial variation of current – it equals the fraction of the net current contained within the radius r. By definition $F(1) = 1$.

Electron beams in plasmas

The toroidal magnetic field is

$$B_\theta(r) = \mu_o I F(r/r_o)/2\pi r. \tag{12.120}$$

The radial equation of motion for an electron with kinetic energy $(\gamma_o\text{-}1)m_e c^2$ and zero angular momentum is

$$\frac{d^2 r}{dt^2} = -\frac{e v_z \mu_o I F(r/r_o)}{2\pi \gamma_o m_e r} . \tag{12.121}$$

If the magnetic field does not vary in time the kinetic energy of an electron is constant. As a result, the axial velocity is related to the radial velocity by:

$$v_z = c\,(\beta_o^2 - v_r^2/c^2)^{1/2}. \tag{12.122}$$

The quantity β_o equals the total velocity divided by c:

$$\beta_o = (1\text{-}1/\gamma_o^2)^{1/2}. \tag{12.123}$$

We can simplify Eqs. (12.121) and (12.122) with the dimensionless variables: $R = r/r_o$, $V_R = v_r/\beta_o c$, $V_Z = v_z/\beta_o c$ and $\tau = t/(r_o/v_o)$. Substituting $\mu_o = 1/\epsilon_o c^2$ the electron equations of motion are:

$$dR/d\tau = V_R, \tag{12.124}$$

$$\frac{dV_R}{d\tau} = -\frac{I}{[4\pi\epsilon_o m_e c^3 \beta_o \gamma_o/e]} \frac{2V_Z F(R)}{R} , \tag{12.125}$$

and

$$V_Z = (1 - V_R^2)^{1/2}. \tag{12.126}$$

The bracketed quantity in the denominator of Eq. (12.125) is the Alfven current:

$$I_A = 4\pi\epsilon_o m_e c^3 \beta_o \gamma_o/e. \tag{12.127}$$

A single parameter (I/I_A) governs the solutions of Eqs. (12.124), (12.125) and (12.126). Figure 12.19 illustrates numerical solutions for a uniform current density, $F(R) = R^2$. When $(I/I_A) \ll 1$ the radial velocity is much smaller than the axial velocity, $V_R \ll V_Z$ (Figure 12.19*a*). In this limit, particle orbits at all radii are almost harmonic. At higher values of (I/I_A), the oscillations of peripheral electrons are anharmonic (Figure 12.19*b*). When the net current equals the value $I = I_A$

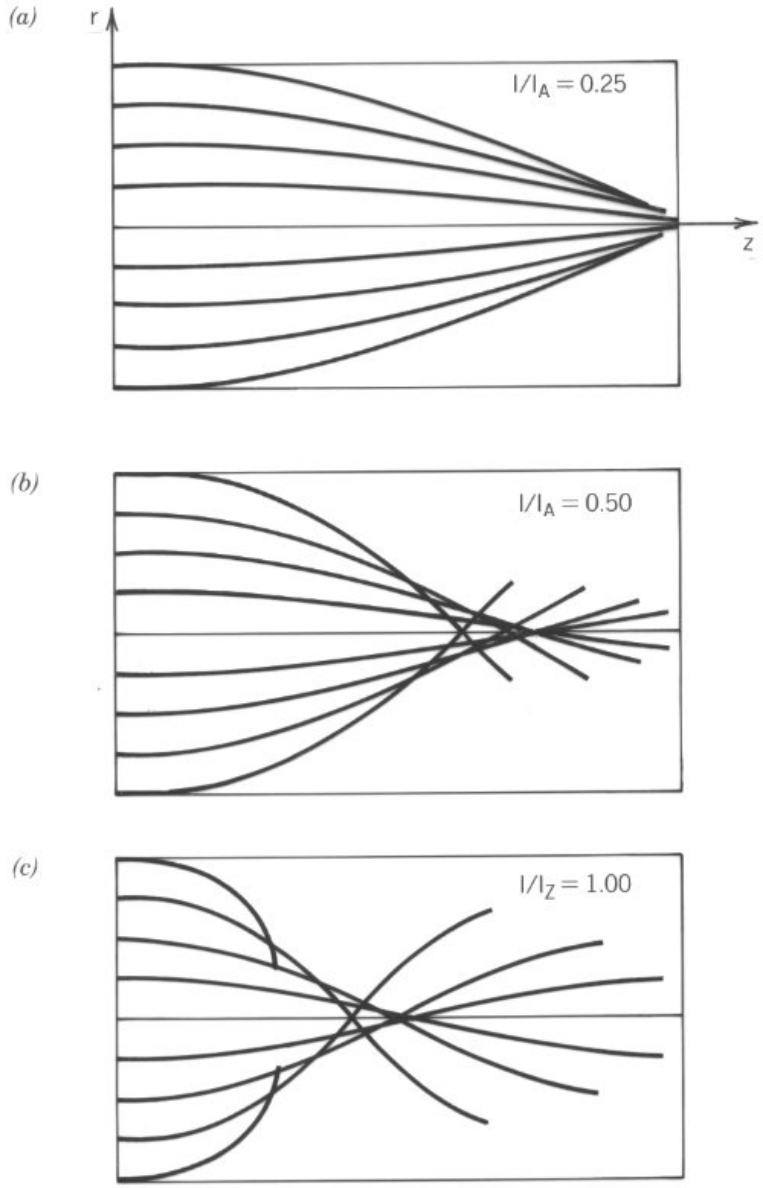

Figure 12.19. Numerical calculations of single electron orbits in the toroidal magnetic field generated by a uniform current density beam. Beam current: I, Alfven current: I_A. *a*) $I/I_A = 0.25$. *b*) $I/I_A = 0.50$. *c*) $I/I_A = 1.00$.

the orbits of the outermost particles bend completely inward, reaching $V_Z = 0$ on the axis (Figure 12.19*c*). A higher current is impossible because it leads to electrons that travel backward along the axis.

If an electron beam with current I_o propagates in an equal density of ions there is no net electric field but there is a magnetic field because the return current of ions is small. In this

instance the Alfven current is the limit on the beam current, $I_o \le I_A$. If the beam propagates in a dense plasma the net current may be smaller than I_o, allowing transport of beam current substantially above I_A. In this case we say that the beam propagates beyond the Alfven limit.

For electrons we can write the Alfven current in practical units as

$$I_A = (17 \times 10^3)\, \beta_o \gamma_o .\ (\mathrm{A}) \quad [\mathrm{Electrons}] \tag{12.128}$$

As an example, the limiting current for a 1.5 MeV electron is about 65 kA. The limiting current for ions is much higher. The Alfven current for an ion with charge state Z and atomic number A is:

$$I_A = (31 \times 10^6)\, (A/Z)\, \beta_o \gamma_o .\ (\mathrm{A}) \quad [\mathrm{Ions}] \tag{12.129}$$

The Alfven current for 2 MeV protons is 2 MA. The limit is an important concern for space-charge-neutralized light-ion beams leaving magnetically insulated diodes (Section 8.8). These beams can generated high magnetic fields because the applied fields prevent axial electron motion.

The radial distribution of current density $F(r/r_o)$ affects the value of the limiting current. A beam with an annular cross section can carry higher current than a solid beam. Figure 12.20 illustrates solutions to Eqs. (12.124), (12.125) and (12.126) for an annular beam. The current density is uniform between r_o and $r_i = 0.667 r_o$. Note that the beam can carry current higher than I_A without reversal of peripheral electron orbits. Regarding the calculation of an annular beam equilibrium it is clear than the orbits of Figure 12.20 are not consistent with the assumed annular profile because they cross the axis. We can resolve the problem by including electrons with non-zero angular momentum. Electrons with the proper angular momentum oscillate in the region between r_i and r_o.

The *Budker parameter* is also used to characterize the effect of beam-generated forces on transverse dynamics. It is closely related to the Alfven current. Consider a cylindrical electron beam of radius r_o. The electrons have total kinetic energy $(\gamma_o - 1) m_e c^2$, average energy $(\gamma - 1) m_e c^2$, total velocity $\beta_o c$ and average axial velocity βc. The quantity N is the total number of electrons per unit length in the axial direction, or

$$N = \int_0^{r_o} 2\pi r dr\ n_e(r). \tag{12.130}$$

The dimensionless Budker parameter (denoted ν) is the product of N times the classical radius of the electron:

$$\nu = N r_e, \tag{12.131}$$

where

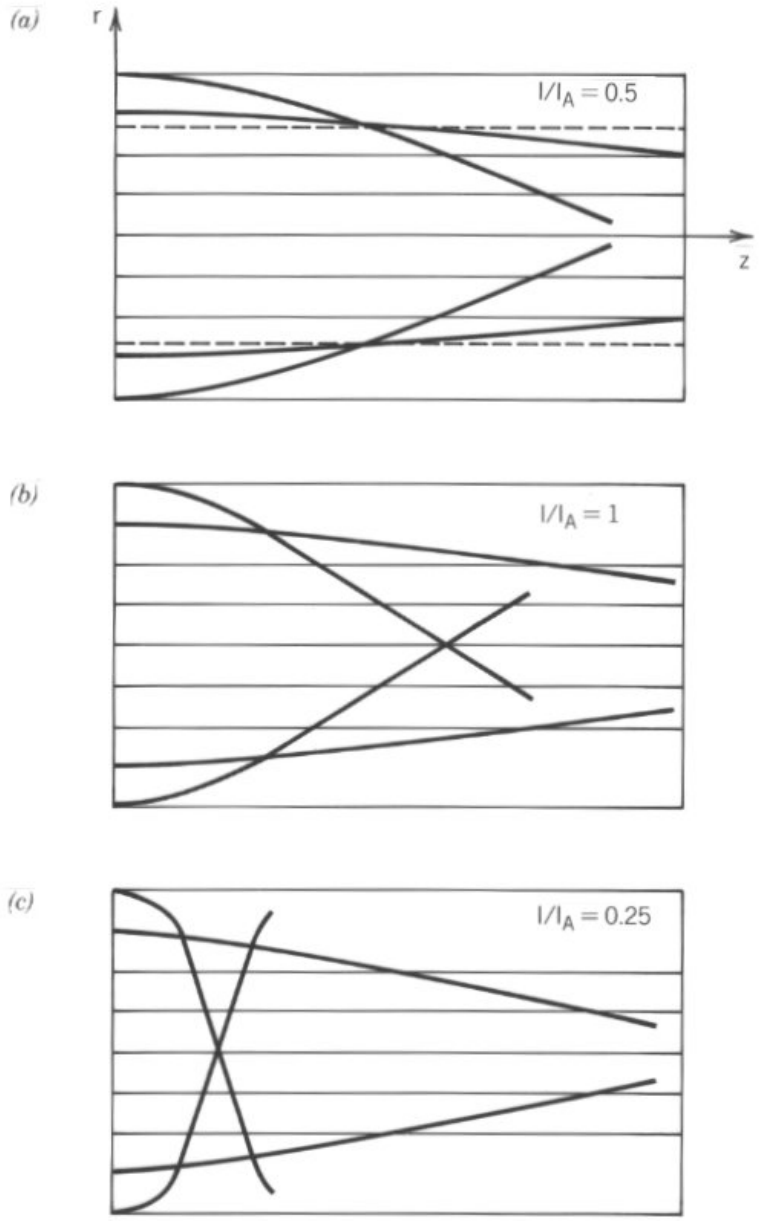

Figure 12.20. Numerical calculations of single electron orbits in the toroidal magnetic field generated by a beam with an annular radial distribution of current density. Dashed line shows assumed inner radius of annular beam. *a*) $I/I_A = 0.50$. *b*) $I/I_A = 1.00$ *c*) $I/I_A = 2.50$.

$$r_e = e^2/4\pi\epsilon_o m_e c^2. \tag{12.132}$$

If βc is the average axial velocity of electrons in a beam, the beam current equals $I_o = eN\beta c$. The Budker parameter is related to the Alfven current by:

$$\frac{\nu}{\gamma} = \frac{e^2 N}{4\pi\epsilon_o m_e c^2 \gamma} = \left[\frac{I_o}{I_A}\right]\left[\frac{\gamma_o \beta_o}{\gamma\beta}\right]. \qquad (12.133)$$

The second factor in brackets on the right-hand side of Eq. (12.133) is close to unity unless the beam propagates near the Alfven current limit. A beam with high ν/γ carries a current close to I_A. If an unneutralized relativistic electron beam has a value of ν/γ close to unity, the difference in electrostatic potential between the axis and the beam envelope is comparable to the average longitudinal kinetic energy:

$$\nu/\gamma \cong e\Delta\phi/\gamma m_e c^2. \qquad (12.134)$$

The implication of Eqs. (12.133) and (12.134) is that the electrons in beams with high ν/γ have substantial transverse energy. Conversely the condition $\nu/\gamma \ll 1$ implies that orbits of the beam electrons are paraxial.

12.8. Bennet equilibrium

The well-known Bennet model [W.H. Bennet, Phys. Rev. **45**, 890 (1934)] describes the self-consistent transverse equilibrium of an intense electron beam propagating through a dense plasma background. The model gives an accurate representation of beams observed in experiments because it incorporates a realistic transverse velocity distribution. The Bennet equilibrium is a good starting point for studies of beam stability.

Suppose a high-energy electron beam travels through a plasma with no externally-applied forces. If the plasma density is much greater than that of the beam the beam drives out plasma electrons to achieve almost complete space-charge neutralization. The only radial forces we need consider are the beam-generated magnetic force and the emittance force from the transverse velocity spread of the beam particles. We seek conditions for a *self-pinched electron beam* where the magnetic and emittance forces balance. To simplify the model, assume that there is no plasma return current and that the current of the cylindrical beam is much smaller than the Alfven current,

$$I_o \ll I_A. \qquad (12.135)$$

The condition of Eq. (12.135) specifies that electron orbits in the beam are paraxial – we can treat transverse and axial motion independently. If all electrons have about the same kinetic energy ($T_e = (\gamma\text{-}1)m_e c^2$) and longitudinal velocity ($v_z = \beta c$) we can use non-relativistic equations with an adjusted electron mass ($m = \gamma m_e$) to describe transverse motion.

In the model the electrons have a Maxwell distribution of transverse velocity with uniform temperature. The condition of uniform temperature means that the shape of the velocity distribution is the same at all positions. If the transverse velocity distribution is isotropic, the

Electron beams in plasmas

Maxwell distribution has the form [Eq. (2.59)]:

$$g(v_x, v_y) = \left[\frac{2m}{\pi kT}\right] \exp\left[\frac{-m_e\,(v_x^2+v_y^2)}{kT}\right]. \tag{12.136}$$

The temperature in Eq. (12.136) is related to the transverse velocity spread of the beam by

$$kT = \gamma m_e \langle v_x^2 \rangle = \gamma m_e \langle v_y^2 \rangle. \tag{12.137}$$

We seek a variation of beam density $n(r)$ that gives force balance at all radii. From the discussion of Section 2.11 the force acting on a Maxwell beam distribution determines the equilibrium density of particles. For a net radial focusing force $F_r(r)$ and a density n_o on the axis, Eq. (2.131) implies that the density is:

$$\frac{n(r)}{n_o} = \exp\left(\int_0^r \frac{F_r(r')dr'}{kT}\right). \tag{12.138}$$

The radial force in Eq. (12.138) results from the beam-generated toroidal magnetic field, $B_\theta(r)$. If all electrons have the same value of βc then the radial magnetic force is:

$$F_r(r) = -e\beta c\, B_\theta(r). \tag{12.139}$$

If we define $I(r)$ as the total axial beam current contained with the radius r, the toroidal magnetic field is:

$$B_\theta(r) = \mu_o I(r)/2\pi r. \tag{12.140}$$

For uniform βc the included current is related to the beam density by:

$$I(r) = \int_0^r 2\pi r' dr'\; e\beta c\; n(r'). \tag{12.141}$$

We can combine Eqs. (12.138) through (12.141) into a single equation that gives the self-consistent equilibrium density of a pinched electron beam:

$$\frac{n(r)}{n_o} = \exp\left(\left[\frac{-1}{kT}\right]\int_0^r dr' \frac{e\beta c\mu_o}{2\pi r'}\int_0^{r'} dr''2\pi r'' e\beta c n(r'')\right). \tag{12.142}$$

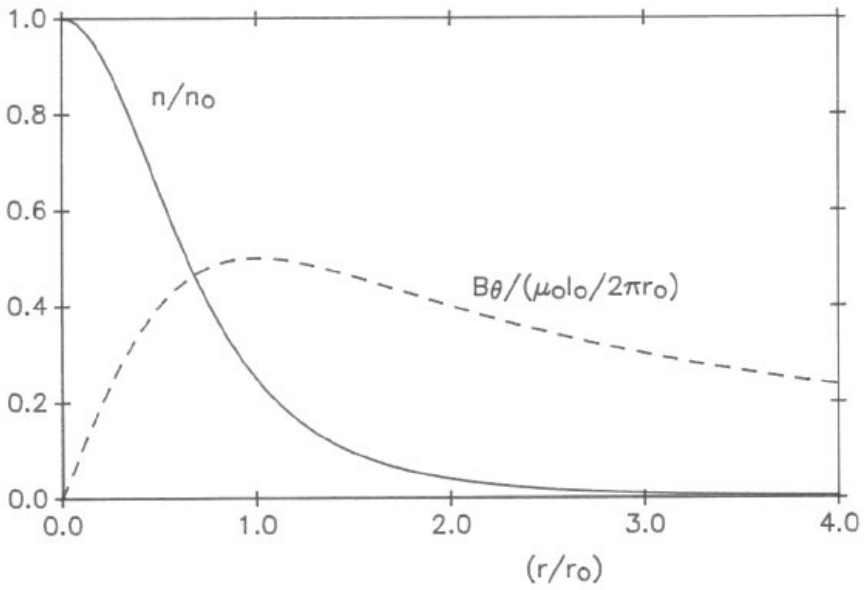

Figure 12.21. Radial variation of the normalized density and toroidal magnetic field for an electron beam in a Bennet equilibrium.

We shall see that Eq. (12.142) holds if the density has the radial variation:

$$n(r) = \frac{n_o}{[1+(r/r_o)^2]^2} \ . \tag{12.143}$$

The quantity r_o is a scaling radius. Substituting from Eq. (12.143) and defining the quantity $\chi = r/r_o$ we can rewrite Eq. 12.142 as:

$$\frac{1}{[1+\chi^2]^2} = \exp\left(\left[\frac{-e^2\beta^2c^2\mu_o\, n_o\, r_o^2}{kT}\right]\int_0^{\chi}\frac{d\chi'}{\chi'}\int_0^{\chi'}\frac{\chi''d\chi''}{(1+\chi^2)^2}\right) \ . \tag{12.144}$$

Carrying out the double integral of Eq. (12.144) leads to the relationship:

$$\frac{1}{[1+\chi^2]^2} = \exp\left(\left[\frac{e^2\beta^2c^2\mu_o\, n_o\, r_o^2}{8kT}\right][-2\ ln(1+\chi^2)]\right) \ . \tag{12.145}$$

Equation (12.145) holds if the first bracketed quantity on the right-hand side equals unity. This equilibrium constraint is called the *Bennet pinch condition*. We can write the Bennet condition

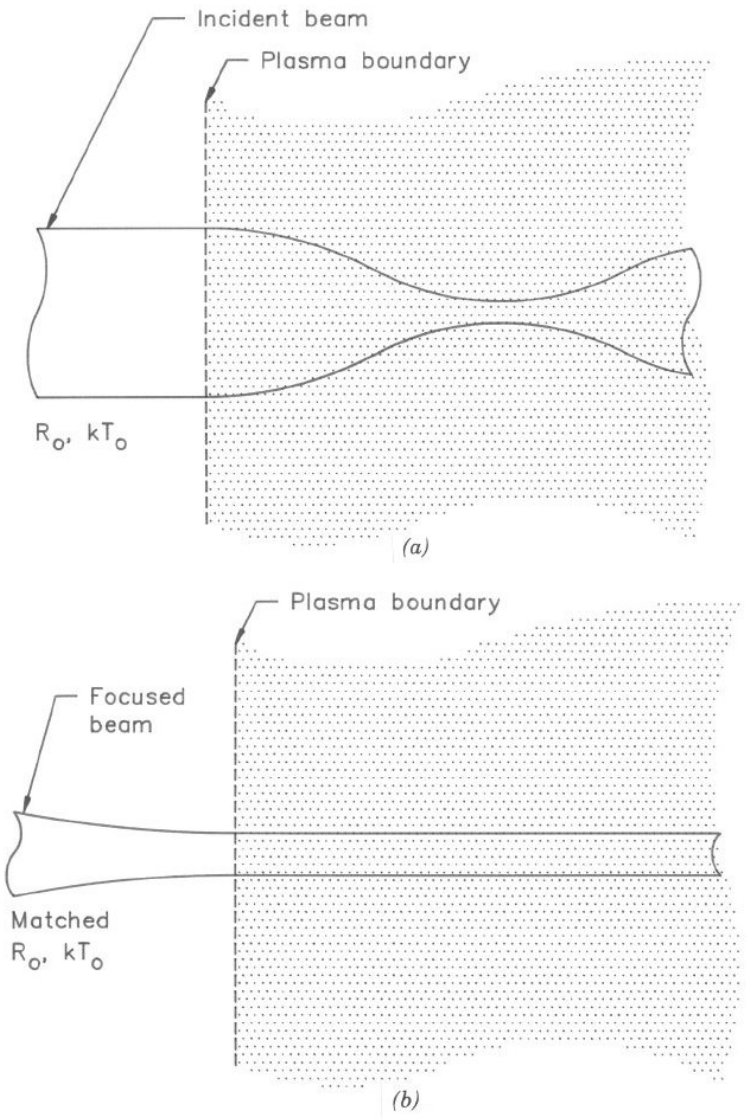

Figure 12.22. Matched propagation of a magnetically-pinched beam in a plasma. *a*) The electron transverse energy spread (kT_o) is too low, resulting in over-focusing and envelope oscillations. *b*) Matching a beam at the plasma boundary by preliminary focusing.

conveniently in terms of the total beam current:

$$I_o = \int_0^\infty 2\pi r dr\ n(r). \tag{12.146}$$

Evaluating Eq. (12.146) for the density expression of Eq. (12.143) gives

$$I_o = (\pi r_o^2)\, e n_o \beta c. \tag{12.147}$$

A familiar form of the Bennet pinch condition is:

$$kT = I_o e \beta c \mu_o / 8\pi. \tag{12.148}$$

We can substitute the Alfven current to derive an alternative form of Eq. (12.148):

$$kT = (I_o/I_A)\, [\gamma m_e (\beta c)^2/2]. \tag{12.149}$$

Equation (12.149) implies that the ratio of the transverse beam energy to the longitudinal energy is roughly equal to the ratio of I_o to I_A.

To this point, we have concentrated on the mathematics of the Bennet model. We can understand the physical meaning of the derivation by verifying that the density of Eq. (12.143) guarantees a balance between the pressure force and magnetic force at all radii. The moment equation for momentum balance [Eq. (2.117)] in an equilibrium beam has the form:

$$kT\, [dn(r)/dr] = -\, e\beta c\, n(r)\, B_\theta(r). \tag{12.150}$$

The left-hand side is the force density associated with a velocity spread while the right-hand side is the magnetic force per volume. We find B_θ by substituting Eq. (12.143) in Eqs. (12.140) and (12.141):

$$B_\theta(r) = (\mu_o I/2\pi r)\, (r/r_o)^2/[1+(r/r_o)^2]. \tag{12.151}$$

Using the expressions of Eq. (12.143) and (12.151), the reader can show that Eq. (12.151) holds at all radii if I_o and kT satisfy the Bennet condition. Figure 12.21 plots the normalized density and magnetic field as a function of (r/r_o). The smooth bell-shaped density profile is a good representation for beams with particles that collide with a background medium.

We have not yet discussed how to calculate the scaling radius r_o. The Bennet equilibrium condition does not depend on r_o. To define the radius we must include information on the distribution of the injected beam. Figure 12.22*a* shows a beam entering a plasma with total current I_o, injection radius R_o and an emittance characterized by kT_o. If kT_o equals kT of Eq. (12.148) the beam is in equilibrium and propagates with $r_o = R_o$. On the other hand if $kT_o < kT$ the beam experiences a focusing force in the plasma that leads to decreased radius. In turn, the two-dimensional beam compression leads to increased transverse temperature (Section 3.8). At some value of reduced radius the pressure force is high enough to reverse the beam compression. The unbalanced non-linear forces cause envelope oscillations and emittance growth. The best approach for plasma transport is to compress the beam reversibly so that it enters the plasma with a matched distribution:

$$kT_o = kT. \tag{12.152}$$

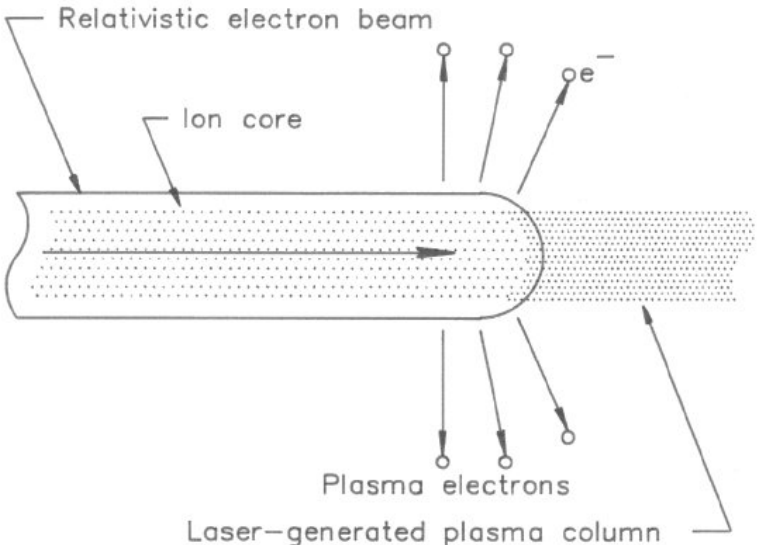

Figure 12.23. Guiding a high-current electron beam by laser generation of a low-density plasma column.

Figure 12.22*b* illustrates matching a beam into a plasma transport channel with a linear lens. The quantity R_o in Figure 12.22*b* is the beam radius consistent with Eq. (12.148).

12.9. Propagation in low-density plasmas and weakly-ionized gases

In this section we shall discuss two examples of high-energy electron beam propagation through a medium. The first topic is laser-guiding of electron beams by selective ionization of a low-density gas. This propagation mode has potential application to high-current electron transport in accelerators. The second topic is the propagation of a self-contained electron beam a long distance through a weakly-ionized gas. This propagation mode is the basis of recurring proposals for electron beam weapons. Our derivation has an educational purpose – we shall see how to add collisional effects to the paraxial envelope equation.

Figure 12.23 shows the idea of electron beam guiding by a laser. A high-power dye laser tuned to a resonance of a low-density background gas generates an extended, narrow channel of plasma. The plasma ion density n_i is much smaller than the beam density n_b. The space-charge fields of an entering relativistic electron eject the low-energy plasma electrons leaving a low-density core of ions. When $n_b > n_i$ the beam expels all plasma electrons. Without electrons there is negligible return current in the beam volume. With sufficient ion density the electron beam can propagate long distances focused by its own magnetic field. We saw in Section 5.5 that the ion density must be in the range

$$1/\gamma^2 < n_i/n_b < 1. \qquad (12.153)$$

for a pinched beam equilibrium. The exact value of density depends on the beam emittance – for paraxial relativistic beams the required value of n_i is low.

Laser guiding has been applied to high-current beams in induction linear accelerators. The advantage is that the beam propagates through the accelerator in a tight pinch. The compressed beam has a high value of angular divergence and is less susceptible to emittance growth. The beam-generated focusing force varies non-linearly with radius. The resulting spread in the betatron wavelength of the beam electrons reduces the growth-rate for transverse instabilities (Section 13.3). On the other hand there are major problems associated with laser guiding in a high-gradient accelerator. The machine must be filled with a special gas such as benzine. Also plasma electrons may accelerate with the beam. Laser guiding only works for short pulse beams. Confinement in a channel depends on localization of the ion density. The beam must pass through before the plasma ions expand. If the beam creates additional ions there is no preferred propagation axis and a perturbation may send the beam sideways; therefore, the pulse length must be shorter than the average time for collisional ionization of the background gas. Electron beams in plasma channels are also subject to a hose instability – Section 13.6 discusses this topic.

We next proceed to electron beam propagation in a weakly-ionized gas. In contrast to the previous model the plasma for beam neutralization is created by the beam through collisional ionization. Usually the plasma density is much higher than that of the beam. In the dense plasma, the electrons have low-temperature and the resistivity is high. Following the discussion of Section 12.6 the plasma return current spreads over a large cross-section, allowing self-pinched beam propagation.

Our goal is to modify the paraxial envelope equation to include collisions that change the axial and transverse momentum of electrons. We shall concentrate on the equilibrium properties of beams – the theory of electron beam stability in a dense gas is a complex and open-ended field. We shall adopt some simplifying assumptions:

1) The paraxial beam has cylindrical symmetry.

2) We limit attention to an envelope model that describes the root-mean-square beam radius $R(z)$ without addressing detailed momentum balance over the cross section.

3) Partial ionization of a background gas provides complete space-charge neutralization of the beam.

4) The magnetic diffusion time is much shorter than the beam pulse length. In the resistive plasma, only a small fraction of the return current flows within the beam volume.

5) There are no applied focusing or acceleration forces.

A set of differential equations describes the beam trace $R(z)$. Although we shall not derive detailed numerical solutions, it is informative to list the equations along with their physical motivation. The first equation defines the envelope angle:

$$dR/dz = R'. \tag{12.154}$$

The cylindrical envelope equation [Eq. (9.25)] gives the change in R' with z:

$$\frac{dR'}{dz} = -\frac{(d\gamma/dz)\,R'}{\beta^2\,\gamma} - \frac{I_o}{I_A\,R} + \frac{\epsilon^2}{R^3}\,. \tag{12.155}$$

The quantities $\gamma(z)$ and $\beta(z)$ are the relativistic parameters of the beam electrons at position z averaged over radius. The first term on the right-hand side of Eq. (12.155) represents the effect of deceleration. We include it because the beam loses energy in collisions with the gas atoms. Because the gas density is almost independent of the beam density we can treat γ' as a given function of z:

$$d\gamma/dz = [(dE/dz)_c + (dE/dz)_r]/m_e c^2. \tag{12.156}$$

Section 10.4 gives expressions for the collisional and radiative stopping powers.

The second term in Eq. (12.156) is the focusing force of the beam magnetic field. The quantity I_o is the total beam current and I_A is the Alfven current [Eq. (12.127)]. With no absorption of beam electrons I_o is almost constant in z. If atomic or nuclear collisions cause the loss of a significant fraction of the beam we can express the current as a given function of z, $I_o(z)$.

The third term represents defocusing by emittance. Although the emittance term has the same form as Eq. (3.42) we recognize that ϵ varies with z. The rate of emittance increase with z depends on $R(z)$, even though single-particle scattering process are uniform throughout the homogenous medium. Because the change in ϵ depends on the beam geometry we must develop a separate differential equation. We can write ϵ^2 in Eq. (12.155) as the product of the mean-squared radius and the mean-squared divergence angle:

$$\epsilon^2 = R^2\langle\theta^2\rangle. \tag{12.157}$$

We define the emittance equation by taking the total derivative of Eq. (12.157), noting that changes in $\langle\theta^2\rangle$ result from both scattering collisions and beam deceleration.

$$\frac{d(\epsilon^2)}{dz} = R^2\langle\theta^2\rangle\left[\frac{2}{R}\frac{dR}{dz} + \left[\frac{1}{\langle\theta^2\rangle}\frac{d\langle\theta^2\rangle}{dz}\right]_c + \frac{2\gamma}{\gamma^2-1}\frac{d\gamma}{dz}\right]. \tag{12.158}$$

The second term in brackets represents the variation in $\langle\theta^2\rangle$ from collisions – Eq. (10.62) gives the derivative. The third term states that normalized emittance is conserved (Section 3.4) if there are no collisions.

We can calculate numerical solutions for the variation of beam envelope by advancing Eqs. (12.154), (12.155) and (12.158) simultaneously from given initial conditions. An analytic solution is possible if we neglect collisional energy loss compared to scattering. This assumption

often holds for moderate-energy electron beams in air or other gases with intermediate to high atomic number. With constant γ, the envelope equation is:

$$\frac{dR'}{dz} = \frac{\epsilon^2}{R^3} - \frac{I}{I_A R} . \tag{12.159}$$

If the beam expansion takes place over a long distance the envelope angle and its derivative are small – the beam is always close to a radial force equilibrium. The two terms on the right-hand side of Eq. (12.159) are almost equal. Using Eq. (12.157) the emittance satisfies the following condition at all values of z:

$$<\theta^2> \cong I_o/I_A. \tag{12.160}$$

For constant I_o Eq. (12.160) states that the angular divergence of electrons in the beam is constant, despite scattering collisions. In response to collisions the beam radius expands to maintain a constant value of $<\theta^2>$.

We can describe the expansion of the beam mathematically. Over a differential distance Δz collisions increase the angular divergence of electrons by an amount

$$\Delta<\theta^2> = (d<\theta^2>/dz)_c \, \Delta z. \tag{12.161}$$

A beam with enhanced angular divergence is not in a radial force equilibrium. The beam must expand to reduce the divergence by an amount $-\Delta<\theta^2>$. According to Section 3.8 the relationship between divergence angle and beam radius for a differential expansion is:

$$\Delta<\theta^2>/<\theta^2> = -2 \, \Delta R/R. \tag{12.162}$$

Substituting from Eqs. (12.160) and (12.161) we find the following equation for the beam radius:

$$\frac{2}{R}\frac{dR}{dz} = \frac{(d\theta/dz)|_c}{(I/I_A)} . \tag{12.163}$$

Integration of Eq. (12.163) gives the Nordsieck equation for expansion of a beam colliding with a background:

$$\frac{R(z)}{R_o} = \exp\left[\frac{<\theta^2>_c}{2(I/I_A)}\right] . \tag{12.164}$$

Note that the quantity $<\theta^2>_c$ in Eq. (12.164) is not the angular divergence of the beam. According to Eq. (12.160) the beam divergence $<\theta^2>$ is constant. Instead $<\theta^2>_c$ is the mean

squared divergence angle that *single electrons* would gain moving a distance z. The mean-squared divergence angle is a function of z. At $z = 0$, $\langle\theta^2\rangle_c = 0$ and $R = R_o$.

As an application example consider a self-pinched beam with $I_o = 5$ kA and $(\gamma\text{-}1)m_e c^2 = 50$ MeV that moves through air at a pressure of 1 mtorr. Equation (12.127) shows that $I_A = 1.6$ MA. Electron motion is paraxial – the ratio (I_o/I_A) equals 3×10^{-3}. Following Eq. (10.62) the mean-squared divergence angle for an equilibrium beam is:

$$(\langle\theta^2\rangle)^{1/2} = 55 \text{ mrad } (3°).$$

Suppose the beam enters the medium with small envelope radius ($R_o = 1$ mm) and the envelope radius at the target must be less than 0.1 m. Equation (12.164) implies that the change in single-particle mean-squared divergence angle is:

$$\langle\theta^2\rangle_c \leq 2(I/I_A)\ln(100) = 2.76 \times 10^{-2}.$$

Inserting the value into Eq. (10.62) with Z = 7 and $N = 7.0 \times 10^{22}$ m^{-3} gives a propagation length of 7.5×10^4 m (75 km). Over this length Eqs. (10.52) and (10.55) predict an energy loss of 18 MeV - the assumption of constant electron energy is marginal.